COMBINED METABOLIC AND CELL POPULATION MODELING FOR YEAST BIOREACTOR CONTROL

Michael A. Henson * **Dirk Müller** **
Matthias Reuss **

* *Department of Chemical Engineering, University of Massachusetts, Amherst, MA 01003, USA*
** *Institute of Biochemical Engineering, University of Stuttgart, 70569 Stuttgart, Germany*

Abstract: Several investigators recently have explored the use of cell population balance equation (PBE) models for the design of biochemical reactor control strategies. A major disadvantage of the PBE modeling approach is that the incorporation of intracellular reactions needed to accurately describe cellular processes leads to substantial computational difficulties. We investigate an alternative modeling technique in which the cell population is constructed from an ensemble of individual cell models. The average value or the number distribution of any intracellular property captured by the cell model can be computed from ensemble simulation data. To illustrate the basic procedure, a single cell model of yeast glycolytic oscillations is used to construct large cell ensembles for the investigation of cell population synchronization. The potential use of cell ensemble models for bioreactor controller design are discussed.

Keywords: cell metabolism, population balance modeling, bioreactor control.

1. INTRODUCTION

The cell population balance equation (PBE) has been developed to describe heterogeneities in large cell populations (Eakman *et al.*, 1966). Most PBE models are based on a single internal state such as cell age (Hjortso and Nielsen, 1995) or cell mass (Zhu *et al.*, 2000). Cell PBE models with a vector of internal states corresponding to intracellular concentrations also can be constructed. The incorporation of intracellular reactions within the PBE framework is facilitated by utilizing a distribution function that represents the mass fraction of cells with a particular internal state (Nielsen and Villadsen, 1994). In addition to difficulties associated with modeling cell cycle events, an inherent limitation of the mass fraction PBE formulation is that a detailed intracellular description leads to a computationally intractable model due to the high dimension of the internal cell state.

Shuler and co-workers (Ataai and Shuler, 1985; Kim and Shuler, 1990; Schuler and Domach, 1983) have developed an alternative modeling approach for heterogeneous cell populations. Rather than formulate the governing PBE, the cell population is described by an ensemble of single cell models which differ according to key properties such as the division size. The number distribution function with respect to any property captured by the single cell model can be calculated from ensemble simulation data. Ensembles with approximately 250 individual cells have been used to predict steady-state and transient size distributions for aerobic (Schuler and Domach, 1983) and anaerobic (Ataai and Shuler, 1985) continuous

cultures of *E. coli* as well as plasmid instability in a genetically modified *E. coli* strain (Kim and Shuler, 1990). We have not found any recent developments or applications of this promising modeling approach. In this paper, we outline the construction of a cell ensemble model for predicting population synchronization associated with yeast glycolytic oscillations (Henson *et al.*, 2002). The results are used to access the utility of cell ensemble models for bioreactor controller design.

2. YEAST GLYCOLYTIC OSCILLATIONS

Glycolysis is the cellular process by which glucose is metabolized to generate stored energy in the form of ATP. Under certain laboratory conditions oscillations have been observed in glycolytic intermediates and extracellular species. Experimental studies (Ghosh and Chance, 1964) suggest that an autocatalytic reaction in the glycolytic chain is responsible for single cell oscillations. Additional experimental work has focused on characterizing the cellular mechanisms which cause synchronization of individual cells such that they oscillate in phase, thereby producing oscillations at the cell population level. These studies suggest that excreted acetaldehyde is the extracellular species which mediates synchronization (Richard *et al.*, 1996).

2.1 Single Cell Model

A single cell model derived from the glycolytic reaction pathway shown in Figure 1 is used for the computational studies presented in this paper. The following model equations (Wolf and Heinrich, 2000) are obtained for an arbitrary cell i:

$$\frac{dS_{1,i}}{dt} = J_0 - v_{1,i} \tag{1}$$

$$\frac{dS_{2,i}}{dt} = 2v_{1,i} - v_{2,i} - v_{6,i} \tag{2}$$

$$\frac{dS_{3,i}}{dt} = v_{2,i} - v_{3,i} \tag{3}$$

$$\frac{dS_{4,i}}{dt} = v_{3,i} - v_{4,i} - J_i \tag{4}$$

$$\frac{dN_{2,i}}{dt} = v_{2,i} - v_{4,i} - v_{6,i} \tag{5}$$

$$\frac{dA_{3,i}}{dt} = -2v_{1,i} + 2v_{3,i} - v_{5,i} \tag{6}$$

where: S_1, S_2, S_3, S_4, N_2 and A_3 denote the intracellular concentrations of the species shown in Figure 1; J_0 is the flux of glucose into the cell; and J_i is the net flux of acetaldehyde/pyruvate out of the i-th cell. The intracellular reaction rates v_2–v_6 depend linearly on the species involved in each reaction (Wolf and Heinrich, 2000). The reaction rate v_1 includes an additional nonlinear factor that accounts for autocatalytic behavior:

$$v_1 = k_1 S_{1,i} A_{3,i} \left[1 + \left(\frac{A_{3,i}}{K_I}\right)^q\right]^{-1} \tag{7}$$

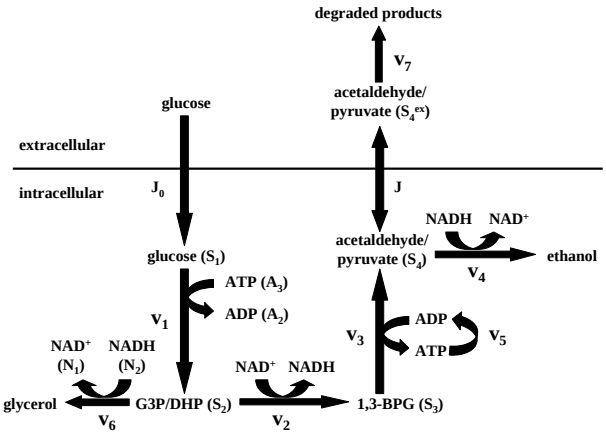

Fig. 1. Yeast glycolysis reaction pathway.

where: k_1, K_I and q are kinetic parameters. The flux of acetaldehyde/pyruvate from the i-th cell into the extracellular environment is modeled as:

$$J_i = \kappa(S_{4,i} - S_{4,ex}) \tag{8}$$

where: $S_{4,ex}$ is the extracellular acetaldehyde/pyruvate concentration; and κ is a coupling parameter related to the cell permeability.

2.2 Cell Population Balance Equation Model

A population balance equation (PBE) model based on the glycolytic reaction network in Figure 1 is formulated to demonstrate the associated computational difficulties. The PBE model is derived using a distribution function that represents the mass fraction rather than the number fraction of cells with a particular internal state because this formalism allows intracellular reactions to be incorporated in a straightforward manner (Nielsen and Villadsen, 1994). The PBE is written as:

$$\frac{\partial \Psi(x,t)}{\partial t} + \sum_{j=1}^{J} \frac{\partial}{\partial x_j} \left[R_j(x,t)\Psi(x,t)\right] = \left[\mu(x,t) - \mu(t)\right] \Psi(x,t) \tag{9}$$

where: x is the internal state vector; $\Psi(x,t)dx$ represents the mass fraction of cells with internal state in the range $[x, x+dx]$ at time t; J is the number of intracellular species; x_j is the intracellular concentration of species j; and $R_j(x,t)$ is the net rate of formation of species j. The function $\mu(x,t)$ represents the specific growth rate of cells with internal state x, while $\mu(t)$ is the average specific growth rate. Both quantities can be calculated directly from the intracellular reaction rates given the associated stoichiometry (Nielsen and Villadsen, 1994). For the yeast glycolytic pathway

depicted in Figure 1, the number of intracellular species $J = 6$ where $x^T = [S_1\ S_2\ S_3\ S_4\ N_2\ A_3]$.

From a computational perspective, the key point is that the internal state x which characterizes the intracellular concentrations of each cell is of dimension six. Assume the model is to be solved numerically by discretization in each of the six internal coordinates (Zhu *et al.*, 2000). This procedure will yield a set of nonlinear ordinary differential equations (ODEs) with time as the only independent variable. If the same number of discretization points m is used for each coordinate, then the total number of ODEs is $n = m^6$. Even with a coarse discretization where $m = 10$, this procedure results in one million ODEs. The dimension of the internal state vector clearly places severe limitations on the complexity of the intracellular reaction network that can be utilized. Furthermore, the mass fraction PBE formalism is not useful for modeling cell cycle events such as budding and mitosis (Nielsen and Villadsen, 1994).

3. CELL ENSEMBLE MODEL

The ensemble modeling technique allows single cell behavior to be described with an appropriate level of detail and circumvents the computational problems inherent in the PBE modeling approach. Furthermore, the number distribution with respect to any property captured by the single cell model can be calculated from ensemble simulation data. Below we construct a cell ensemble model to investigate the synchronization phenomenon associated with yeast glycolytic oscillations.

3.1 Model Formulation and Solution

The dynamics of the i-th cell in the population are represented by (1)–(8). A mass balance on extracellular acetaldehyde/pyruvate is derived under the assumption that the cell volume density (φ) remains constant as the number of cells M is varied (Wolf and Heinrich, 2000):

$$\frac{dS_{4,ex}}{dt} = \frac{\varphi}{M}\sum_{1}^{M} J_i - v_7 = \frac{\varphi}{M}\sum_{1}^{M} J_i - kS_{4,ex} \quad (10)$$

where k is the kinetic constant of the acetaldehyde/pyruvate degradation reaction. The total number of ODEs (n) in the cell ensemble model increases linearly with the number of intracellular species (6) and the number of individual cells (M): $n = 6M+1$. This is to be contrasted with the PBE model (9) where the number of ODEs obtained from discretization increases as the power of the number of intracellular species.

The model parameter values used in the subsequent simulations are identical to those listed in our original paper (Henson *et al.*, 2002). For these values, the cell ensemble model possesses a single stable periodic solution in which all the cells oscillate in phase and with the same amplitude regardless of the cell number. Substantially more complex oscillatory solutions are obtained when each cell is subject to random perturbations in the intracellular kinetic parameters. The dynamic simulation code was developed in FORTRAN using the variable step ODE solver `DVODE` (Brown *et al.*, 1989). Efficient solution of large cell ensembles was achieved by approximating the full Jacobian matrix with a banded Jacobian matrix. The actual Jacobian matrix is not banded due to the presence of the acetaldehyde/pyruvate flux J_i in (4) and (10). When these flux terms are neglected in the Jacobian calculation, the problem becomes highly banded. We found that this simplification reduced computation time by at least an order of magnitude. A typical one hour dynamic simulation with 1000 cells required less than 10 minutes of CPU time on a Pentium III 700 MHz processor.

3.2 Calculation of Distribution Properties

Numerical integration of the cell ensemble model produces a data matrix which contains the intracellular concentrations of each cell and the extracellular acetaldehyde/pyruvate concentration at each sampling point in time. This problem of computing cell size distributions from ensemble data was investigated previously for *E. coli* (Schuler and Domach, 1983). Below we present a simple algorithm for computing the cell number distribution with respect to any intracellular variable.

Let $z(t)$ represent the intracellular variable for which the cell number distribution function $N(z,t)$ is to be calculated. Consider discretization of the internal coordinate z into L intervals of width $\Delta z_l = z_l - z_{l-1}$ where $z_0 = z_{min}$ and $z_L = z_{max}$. By definition of the distribution function:

$$\int_0^\infty N(z,t)dz \cong \sum_{l=1}^{L} N_l(t)\Delta z_l = 1 \quad (11)$$

where $N_l(t)$ represents the average value of $N(z,t)$ over the interval Δz_l. Denote $\tilde{z}_i(t_k)$ as the value of the intracellular variable z produced by the i-th cell at the discrete time t_k. For an ensemble consisting of M individual cells, the mean value of the intracellular variable z at time t_k is:

$$\bar{z}(t_k) = \frac{1}{M}\sum_{i=1}^{M} \tilde{z}_i(t_k) \quad (12)$$

The distribution function is computed by partitioning the ensemble into the discrete intervals:

$$\tilde{n}_l(t_k) = \sum_{i=1}^{M} \{S[\tilde{z}_i(t_k) - z_{l-1}] - S[\tilde{z}_i(t_k) - z_l]\} \quad (13)$$

where: $\tilde{n}_l(t_k)$ represents the number of cells with intracellular state z in the range $[z_{l-1}, z_l)$; $l \in [1, L]$; and $S(x)$ is the unit step function. The discretized approximate number distribution function is calculated as:

$$\tilde{N}_l(t_k) = \frac{\tilde{n}_l(t_k)}{M\Delta z_l}, \qquad l \in [1, L] \tag{14}$$

If the discretization interval is sufficiently small, then a smooth continuous number distribution $\tilde{N}(z, t_k)$ can be computed from the discrete distribution values $\tilde{N}_l(t_k)$ by polynomial interpolation.

Resolution of the population behavior is determined primarily by the number of cells M in the ensemble. As M is increased, the number of intervals L also can be increased such that each interval is populated with a sufficient number of cells to produce a smooth distribution function. If L is chosen too small relative to M, resolution is unnecessarily lost. Conversely, the distribution function will be noticeably non-smooth if L is chosen too large relative to M.

4. SIMULATION STUDY

The cell ensemble modeling approach is applied to the problem of yeast glycolytic oscillations. We focus on NADH concentration dynamics to allow comparisons to experimental data where the average NADH concentration was continuously measured by fluorometry (Ghosh and Chance, 1964; Richard *et al.*, 1996). The ensemble model produces non-trivial number distributions (*i.e.*, cells with different NADH concentrations) only if there is some source of randomness in the individual cell models. Two possible sources of randomness are investigated in the following simulations.

The first test involves an ensemble of 1000 cells in which the initial conditions of each individual cell are perturbed according to a Gaussian distribution with zero mean and a variance of 2.25. Figure 2 shows the NADH concentration evolution of each cell. Due to the large variance used, initially the cell population is disorganized and exhibits no temporal structure indicative of a synchronized culture. A highly synchronized population in which the cells oscillate in phase and with a period of approximately one minute is observed after 60 minutes. Figure 3 shows the ensemble average NADH concentration dynamics and the NADH number distributions computed with $z_0 =$ 0 mM, $z_L = 0.3$ mM and $\Delta z = 0.005$ mM at three times during the simulation. The computed distributions show the presence of two distinct cell subpopulations which eventually become synchronized and converge into a single population that produces fully developed oscillations. Slower synchronization is observed when less cell models are included in the ensemble (Henson *et al.*, 2002).

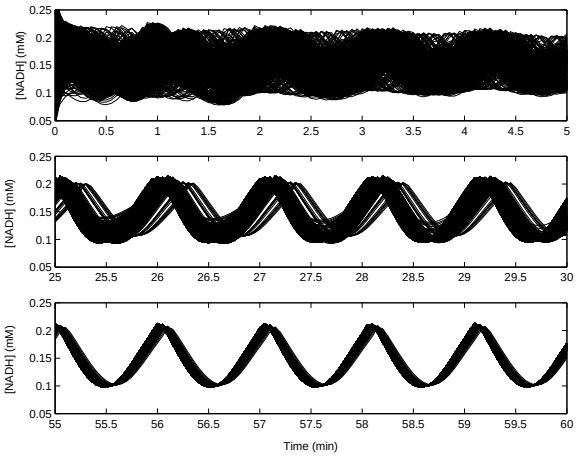

Fig. 2. Cell population synchronization for randomized initial cell state.

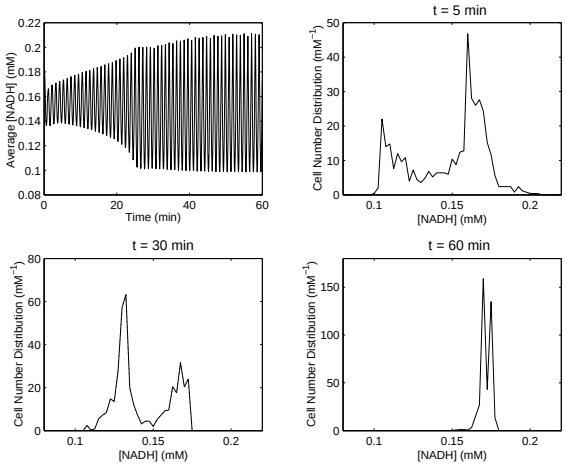

Fig. 3. Ensemble average NADH concentration dynamics and NADH number distributions corresponding to Figure 2.

The next test involves a 1000 cell ensemble in which the intracellular reaction rate parameters of each cell are randomly perturbed with zero mean and variance of 6.25×10^{-4}. Figure 4 shows the evolution of the NADH concentration of each individual cell at the end of a 150 minute dynamic simulation. While the dynamic behavior is not easily characterized, the random variations appear to produce three distinct subpopulations. This behavior is more clearly evident in Figure 5 where the dynamics of the average NADH concentration and the NADH concentration of three individual cells near the end of the 150 minute simulation are shown. The individual cells have been chosen to show the oscillatory dynamics of representative cells from the three subpopulations observed in Figure 4. Each subpopulation must contain a sufficient number of cells to yield accurate predictions of average and distribution properties. This is possible only if the cell ensemble is sufficiently large. The top plot in Figure 6 shows the complete evolution of the average NADH concentration. The bottom plot shows the NADH number distributions computed at at 0 (—), 10 ($\cdots$) and 150 ($- - -$)

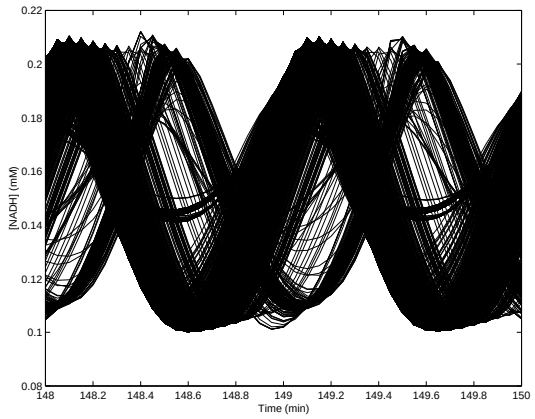

Fig. 4. Cell population dynamics for randomized intracellular kinetic parameters.

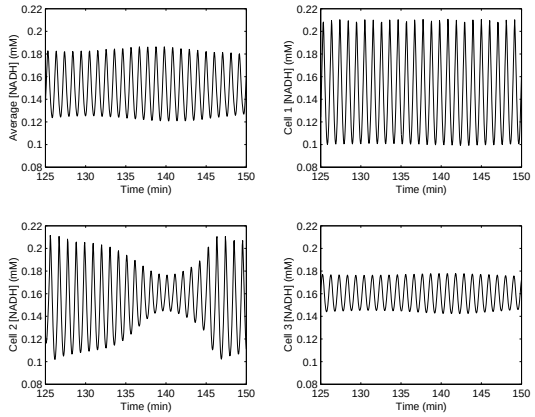

Fig. 5. NADH concentration dynamics for the total ensemble and three representative cells corresponding to Figure 4.

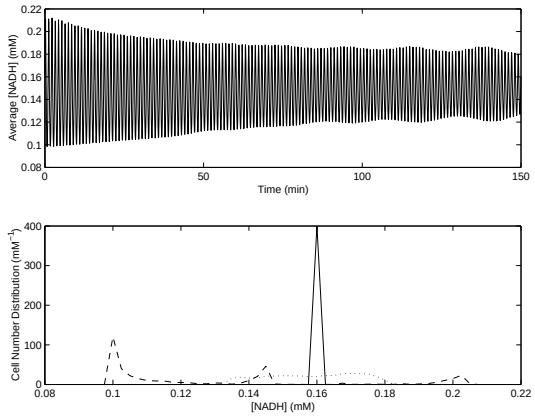

Fig. 6. Ensemble average NADH concentration dynamics and NADH number distributions corresponding to Figure 4.

minutes. The sharp initial distribution is indicative of a highly synchronized cell population. As random cell variations lead to desynchronization, the NADH distribution becomes increasingly dispersed. The final distribution clearly shows the existence of the three distinct cell subpopulations.

5. BIOREACTOR CONTROLLER DESIGN

The cell ensemble modeling approach allows a detailed single cell model to be incorporated within a cell population description. As a result, cell ensemble models are well suited for predicting complex population dynamics observed in biochemical reactors. The development of cell population control strategies based on such detailed models offers the potential to enhance bioreactor productivity, especially with respect to extracellular metabolites that are excreted during a specific phase of the cell cycle as a result of complex interactions between cellular metabolism and cell cycle events (Alberghina *et al.*, 1991).

As compared to simpler modeling techniques commonly used for bioreactor simulation and control (Daoutidis and Henson, 2002), an obvious shortcoming of the cell ensemble approach is model complexity. We have shown that the total number of model equations increases linearly both with the number of equations in the single cell model and the number of cells included the ensemble. However, the simple cell model used in this paper yields an ensemble model of 6000 differential equations. More complex cell models (Domach and Shuler, 1984; Ataai and Shuler, 1985) and/or larger ensembles will yield population models that are difficult to solve efficiently. This raises serious questions about the possible utility of these models for bioreactor control.

Clearly the development of control strategies based on high dimensional cell ensemble models will be facilitated by continuing improvements in computing technology. Parallel advances in single cell modeling and cell ensemble solution algorithms also will be required. For example, judicious simplification of intracellular reaction networks can reduce the computational burden associated with the individual cell model. Only the reaction pathways most relevant to the cellular behavior being studied need be incorporated. Furthermore, linear reaction pathways often can be lumped into a single reaction without loss of model fidelity to reduce the number of dependent variables (Nielsen and Villadsen, 1994). The cell model studied in this paper only contains lumped reactions in the upper part of the glycolytic pathway because this level of detail is sufficient to describe the oscillatory dynamics.

Model complexity also may be reduced by using a relatively small number of single cells to construct the ensemble model. In this paper, we used large ensembles of 1000 cells to achieve fine resolution of the computed cell number distributions. Previous work on *E. coli* suggests that smaller ensembles comprised of a few hundred cell models can be sufficient to resolve the population behavior (Domach and Shuler, 1984; Ataai

and Shuler, 1985). Furthermore, the ensemble size required to achieve satisfactory prediction of cell population dynamics within a feedback control strategy may be considerably less than that needed to generate high fidelity simulation results.

The development of control strategies based on cell ensemble models will require the formulation and solution of large-scale state estimation problems. The first step in this direction is analysis of cell ensemble model observability for given sets of intracellular and extracellular measurements. Extensive distribution measurements of intracellular concentrations that are required to achieve observability typically will not be available. In this case, estimation of unobservable state variables via an open-loop observer should be possible. Regardless of the problem formulation, the nonlinear state estimator will require the development of customized numerical solution techniques. The computation time required to solve the cell ensemble model studied in this paper was reduced by an order of magnitude by exploiting the approximately banded structure of the model equations. The same simplification should be applicable to other ensemble models in which the individual cells interact via a limited number of species in the extracellular environment. For example, cell cycle dependent oscillations observed in continuous yeast bioreactors are believed to be mediated by ethanol excreted into the extracellular environment (Nielsen and Villadsen, 1994).

Despite these possible improvements, cell ensemble models will remain complex and difficult to utilize for model-based control. The incorporation of such models within nonlinear optimization-based control strategies appears to infeasible. We intend to pursue linear model predictive control and simple nonlinear control techniques such as feedback linearization. More specifically, population control strategies will be developed for continuous yeast bioreactors to determine the productivity improvements which result from using an ensemble model based on a detailed single cell model instead of population balance equation model in which the intracellular state is characterized only by cell mass (Zhu *et al.*, 2000).

6. ACKNOWLEDGEMENTS

The first author would like to acknowledge the Alexander von Humboldt Foundation (Germany) for partial financial support of this research.

REFERENCES

Alberghina, L., B. M. Ranzi, D. Porro and E. Martegani (1991). Flow cytometry and cell cycle kinetics in continuous and fed-batch fermentations of budding yeast. *Biotech. Prog.* **7**, 299–304.

Ataai, M. M. and M. L. Shuler (1985). Simulation of CFSTR through development of a mathematical model for anaerobic growth of *Escherichia coli* cell population. *Biotech. Bioeng.* **27**, 1051–1055.

Brown, P. N., G. D. Byrne and A. C. Hindmarsh (1989). VODE: A variable coefficient ODE solver. *SIAM J. Sci. Stat. Comput.* **10**, 1038–1051.

Daoutidis, P. and M. A. Henson (2002). Dynamics and control of cell populations in continuous bioreactors. *AIChE Symposium Series* **326**, 274–289.

Domach, M. M. and M. L. Shuler (1984). A finite representation model for an asynchronous culture of *E. coli*. *Biotech. Bioeng.* **26**, 877–884.

Eakman, J. M., A. G. Fredrickson and H. H. Tsuchiya (1966). Statistics and dynamics of microbial cell populations. *Chem. Eng. Prog. Symp. Ser.* **62**, 37–49.

Ghosh, A. and B. Chance (1964). Oscillations for glycolytic intermediates in yeast cells. *Biochemical and Biophysical Research Communications* **16**, 174–181.

Henson, M. A., D. Muller and M. Reuss (2002). Cell population modeling of yeast glycolytic oscillations. *Biochemical J.* **368**, 433–446.

Hjortso, M. A. and J. Nielsen (1995). Population balance models of autonomous microbial oscillations. *J. Biotech.* **42**, 255–269.

Kim, B. G. and M. L. Shuler (1990). A structured, segregated model for genetically modified *Escherichia coli* cells and its used for prediction of plasmid stability. *Biotech. Bioeng.* **36**, 581–592.

Nielsen, J. and J. Villadsen (1994). *Bioreaction Engineering Principles*. Plenum Press. New York, NY.

Richard, P., B. M. Bakker, B. Teusink, K. van Dam and H. V. Westerhoff (1996). Acetaldehyde mediates the synchronization of sustained glycolytic oscillations in populations of yeast cells. *Eur. J. Biochem.* **235**, 238–241.

Schuler, M. L. and M. M. Domach (1983). Mathematical models of the growth of individual cells. In: *Foundations of Biochemical Engineering* (H. W. Blanch, E. T. Papoutsakis and G. Stephanopolous, Eds.). Chap. 5, pp. 93–133. ACS. Washington D.C.

Wolf, J. and R. Heinrich (2000). Effect of cellular interaction on glycolytic oscillations in yeast: A theoretical investigation. *Biochem. J.* **345**, 321–334.

Zhu, G.-Y., A. M. Zamamiri, M. A. Henson and M. A. Hjortso (2000). Model predictive control of continuous yeast bioreactors using cell population models. *Chem. Eng. Sci.* **55**, 6155–6167.

OPTIMIZATION OF A FED-BATCH BIOREACTOR USING SIMULATION-BASED APPROACH

Catalina Valencia Peroni [*] **Jay H. Lee** [**,1]
Niket S. Kaisare [**]

[*] *Universitat Rovira I Virgili, Tarragona, Catalunya, Spain*
[**] *School of Chemical Engineering, Georgia Institute of Technology, Atlanta, GA 30332, U.S.A.*

Abstract: We use simulation-based approach to find the optimal feeding strategy for cloned invertase expression in *Saccharomyces cerevisiae* in a fed-batch bioreactor. The optimal strategy maximizes the productivity and minimizes the fermentation time. This procedure is motivated from Neuro Dynamic Programming (NDP) literature, wherein the optimal solution is parameterized in the form of a cost-to-go or profit-to-go functions. The proposed approach uses simulations from a heuristic feeding policy as a starting point to generate the profit-to-go vs state data. An artificial neural network is used to obtain profit-to-go as a function of system state. Iterations of Bellman equation are used to improve the profit function. The profit-to-go function thus obtained, is then implemented in an online controller, which essentially converts infinite horizon problem into an equivalent one-step-ahead problem.

Keywords: Fed-batch Reactor, Optimal Control, Neuro-Dynamic Programming

1. INTRODUCTION

A vast majority of industrially important fermentors are operated in fed-batch mode, which involves addition of substrates continuously to an otherwise batch reactor. Fed-batch reactors are especially useful when growth or metabolite production follows substrate or product inhibition kinetics. In such cases, substrates need to be added in a controlled manner in order to maximize the productivity with respect to the desired product. For example, if product formation is inhibited under excess substrate conditions, low substrate concentrations are desired for high product yields. At the same time, higher substrate levels are required to prevent starvation of cells and to maintain high growth rates. Thus, there exists an optimum feed profile that maximizes the productivity of the process.

The determination of optimal feed profile is a challenging problem, as the bioreactors follow complex nonlinear dynamics. Resulting optimal control problem is therefore a nonlinear programming (NLP) problem accompanied by various input and state constraints. The optimization is often non-convex and the global optimum difficult to achieve (Banga *et al.*, 1997).

Many authors have used Pontryagin's maximum principle to solve the optimal control problem. However, this approach may be very difficult for such problems; so several alternative solution techniques have been proposed. Cuthrell and Biegler (1989) solved the optimal control problem of a fed-batch penicillin reactor using successive quadratic programming (SQP) based on orthogonal collocation on finite elements. Luus (1993) used iterative dynamic programming (IDP) to find optimal feed profile for the same reactor; while Banga *et al.* (1997) presented a fast stochastic dynamic optimization method — called in-

[1] The author to whom correspondence should be addressed. Email: jay.lee@che.gatech.edu

tegrated controlled random search for dynamic systems, ICRS/DS — for this reactor. Recently, Bonvin *et al.* (2002) provided a good review of dynamic optimization methods for batch processes, and also presented algorithms that achieve nearly optimal performance in the presence of uncertainties.

In this paper, optimal control of a fed-batch fermentor for cloned invertase expression in *Saccharomyces cerevisiae* is considered. The expression of the enzyme is repressed at high glucose concentration. Hence, a fed-batch reactor is ideal for this process (Patkar and Seo, 1992). Patkar *et al.* (1993) proposed a model for this fermentation process, involving a set of four coupled ODEs. They used first-order conjugate gradient method in order to find the optimal feed rate profile for this system. Later, Chaudhuri and Modak (1998) used a neural network model into the generalized reduced gradient method for the same optimization problem.

The main disadvantage of the above methods is that the fermentation ending time should be fixed a priori in both cases. In order to find the optimal fermentation ending time, several different fermentation ending times should be guessed and, for each one of them, one productivity optimization problem should be solved. This is extremely computationally demanding. Methods such as control parameterization may be used for free-end-time problems to obtain open loop optimal policies. Another drawback of these methods stems from the fact that they are open loop optimal, which means that each time an initial condition changes, a new and different optimization problem should be solved. Besides, the resulting fixed policies do not take into account the possible process disturbances.

Dynamic Programming (DP) is an optimization method that can be used to overcome these limitation. It was introduced by Bellman and coworkers (Bellman, 1957) as a feasible approach to solve the dynamic optimization that results from an optimal control problem. Here, the aim is to find the optimal *'cost-to-go'* function, which can be used to parameterize the optimal solution as a function of the system state. This method is promising as presents a feasible approach to solve any optimal control problem. However, it suffers from *'curse of dimensionality'*, which refers to exponential increase in computational cost with increase in state dimension.

Recently, Neuro-Dynamic Programming (NDP) was proposed as a way to alleviate the curse of dimensionality (Bertsekas and Tsitsiklis, 1996). NDP uses simulated process data obtained under suboptimal policies to fit an approximate cost-to-go function – usually by fitting artificial neural networks, hence the name. The initial approximate cost-to-go function is further improved by an iteration procedure based on the so called Bellman equation. Closely related to NDP are the methods in AI literature, collectively classified as Reinforcement Learning (RL, Sutton and Bartow (1998)). We applied this approach to online control of a continuous bioreactor (Kaisare *et al.*, 2002) as well as that of a benchmark *Van der Vusse* reactor (Lee and Lee, 2001). Simulation-based NDP method will be applied for optimal control of the fed-batch *Saccharomyces cerevisiae* fermentor. We have considered a deterministic optimization problem, i.e. the model is known and full state feedback is assumed. The method can be expanded to stochastic case. Moreover, simulation-based NDP methods do not require the explicit model to be known—methods like Q-learning (Watkins and Dayan, 1992) developed in RL community are model-free stochastic learning techniques.

2. STATEMENT OF THE OPTIMAL CONTROL PROBLEM

Our objective is to find an optimal feed profile μ that adapts itself when initial conditions change or when disturbances occur. The optimal policy is a function of the system state, represented as

$$\mu(x) = \arg\max_{u,t_f} \{productivity - \lambda \cdot t_f\} \quad (1)$$

subject to relevant input and state constraints and following system dynamics. λ is a positive constant that penalizes invertase fermentation time.

In general, the performance index is mathematically represented as the sum of stage-wise costs incurred (or rewards obtained) until the end of horizon.

$$J(x_k) = \sum_{i=k}^{t_f} \phi(x_i, u_i) + \bar{\phi}_t(x_{t_f}) \quad (2)$$

subject to

$$\text{Path Constraint:} \quad g_i(x_i, u_i) \geq 0$$
$$\text{Model Constraint:} \quad \dot{x} = f(x, u)$$

Here ϕ is the stage-wise cost/reward and $\bar{\phi}_p$ is the terminal cost/reward. The path constraints include all input and state constraints. The system dynamics appear as model constraints. For discrete-time system, the model $f(x, u)$ can be integrated for one time step. Equivalently, model constraint becomes $x_{k+1} = f_h(x_k, u_k)$.

The above problem is an infinite-horizon control problem, as we wish to solve free terminal time optimal control (i.e. t_f is not fixed).

3. NEURO-DYNAMIC PROGRAMMING

We begin this section with the description of Dynamic Programming (DP), which is an elegant way to solve the previously introduced optimization problem. In this method, the process is modeled as a chain of consecutive transitions from one state to another. The way each transition is made depends on the decision variable, which has an associated cost or reward. The objective of dynamic programming is to maximize the total profit or minimize the total cost, obtained from the transitions needed to reach the final desired process state from initial process state.

DP involves stage-wise calculation of the *profit-to-go* function [2] to arrive at the solution, not just for a specific x_0 but for general x_0. Thus, the objective function is split into two parts — one stage reward obtained in going from x_k to x_{k+1}, and total future rewards as a function of x_{k+1}. The latter is parameterized as profit-to-go function, which represents the "desirability" of state x_{k+1}. Using the profit-to-go function, the multi-stage optimization problem is cast into an equivalent single-stage optimization that is solved online.

$$\max_{u_k} \{\phi(x_k, u_k) + J^*(x_{k+1})\} \tag{3}$$

where the optimal profit-to-go function is at each stage is defined as

$$J^* = \max_u \left\{ \sum_{i=k+1}^{t_f} \phi(x_i, u_i) + \bar{\phi}_t(x_{t_f}) \right\} \tag{4}$$

The crucial step in DP is calculation of the profit-to-go function $J^*(x)$. This involves stage-wise evaluation of rewards obtained in all possible transitions from each state in the state space. Without going into further details, we mention here that this approach is seldom practically feasible due to the exponential growth of the computation with respect to state dimension. This is referred to as the 'curse of dimensionality', which must be removed in order for this approach to find a widespread use.

An alternative method, which uses simulations to overcome the curse of dimensionality, involves computation of an approximation of the profit-to-go function. Exhaustive sampling of state space can be avoided by identifying relevant regions of the space through simulation under judiciously chosen suboptimal policies. The *policy improvement theorem* states that the new policy defined by $\mu(x) = \arg\max_u \left\{\phi(x,u) + J^i(f_h(x,u))\right\}$ is an improvement over the original policy (Howard, 1960). Indeed, when the new policy is as good as the original policy, the above equation becomes the same as Bellman optimality equation (5).

$$J_\infty(x) = \max_u \{\phi(x,u) + J_\infty(f_h(x,u))\} \tag{5}$$

Equivalently, for a free-end-time batch optimization problem, the above equation can be formulated as

$$J_\infty(x) = \max \left[\bar{\phi}_t(x), \max_u \{\phi(x,u) + J_\infty(f_h(x,u))\}\right] \tag{6}$$

where the modification accounts for termination of batch at a state x. In other words, if $\bar{\phi}_t(x)$ is greater than the second term, the batch should be terminated.

Use of the Bellman equation to obtain iterative improvement of cost-to-go approximator forms the crux of various methods like Neuro-Dynamic Programming (NDP) (Bertsekas and Tsitsiklis, 1996), Reinforcement Learning (RL) (Sutton and Bartow, 1998), Temporal Difference (Tsitsiklis and Roy, 1997) and such.

In this paper, the basic idea from NDP and RL literature is used to obtain optimal performance of a fed-batch bioreactor. Relevant regions of the state space are identified through *simulations* of several heuristic policies, and initial suboptimal profit-to-go function is calculated from the simulation data. A *functional approximator* is used to interpolate between these data points. Neural network is the chosen function approximator (hence the name 'Neuro' in NDP). *Evolutionary improvement* is obtained through iterations of the Bellman equation (7). When the iterations converge, this offline-computed profit-to-go approximation is then used for online optimal control calculation for the reactor.

3.1 *Algorithm*

A detailed algorithm was presented in our previous work (Kaisare *et al.*, 2002), which is reproduced in this section. Following notations are used in this section and rest of the paper. J represents profit-to-go values. A function approximation relating J to corresponding state x is denoted as $\tilde{J}(x)$. Superscript $()^i$ represents iteration index for cost iteration loop and k is discrete time. Finally, $\tilde{J}(k) \equiv \tilde{J}(x(k))$ and $\phi(k) \equiv \phi(x(k), u(k))$.

The simulation-based approach involves computation of the converged profit-to-go approximation offline. The following steps describe the general procedure for the infinite horizon profit-to-go approximation.

[2] It is customary in DP to use cost-to-go for minimization problem. We use profit-to-go as we solve maximization problem. Both cost and profit are exactly equivalent

(1) Perform simulations of the process with chosen suboptimal policies under all representative operating conditions.
(2) Using the simulation data, calculate the ∞-horizon profit-to-go for each state visited during the simulation. For example, each closed loop simulation yields us data $x(0), x(1), \ldots, x(t_f)$, where t_f is the termination time for the specific suboptimal policy. For each of these points, compute the profit-to-go value.
(3) Fit a neural network or other function approximator to the data to approximate the profit-to-go function — denoted as $\tilde{J}^0(x)$ — as a smooth function of the states.
(4) To improve the approximation, perform the following iteration (referred to as the cost or value iteration) until convergence:
    - With the current profit-to-go approximation $\tilde{J}^i(x)$, calculate $J^{i+1}(k)$ for the given sample points of x by solving

$$J^{i+1} = max\left[\bar{\phi}_t(x_k) \max_u \{\phi(x_k, u_k) + \tilde{J}^i(f_h(x_k, u_k))\}\right] \quad (7)$$

      which is based on the Bellman Equation.
    - Fit an improved cost-to-go approximator $\tilde{J}^{i+1}$ to the x vs. $J^{i+1}(x)$ data.
(5) **Policy Update** may sometimes be necessary to increase the coverage of the state space. In this case, more suboptimal simulations with the updated policy ($\max_u \phi + \tilde{J}^i$) are used to increase the coverage or the number of data points in certain region of state space.

Once the value iteration described above converges, the resulting profit-to-go function can be used for online control. At each time, state estimates are obtained (for deterministic problem, we have the state itself). Single-stage optimization problem, as shown in Eq. (3), is solved using the converged profit-to-go function $\tilde{J}_a$ in place of the optimal J^*.

4. INVERTASE PRODUCTION OPTIMIZATION

The fermentation process considered here consists of production of invertase in *Saccharomyces cerevisiae* utilizing glucose for growth. Patkar and Seo (1992) reported the fermentation kinetics of invertase production in fed-batch cultures; as well as experimental data for cell density (c, expressed as optical density OD), glucose concentration (s gm/L) and specific invertase activity (i) obtained with various glucose feeding strategies in 1.2 liter bioreactor. The productivity of the reactor at any time is given by

$$productivity = icV \quad (8)$$

Thus the optimization problem as defined in Eq. (1) becomes

$$\max_{u,t_f} \left\{ icV|_{t_f} - \lambda t_f \right\} \quad (9)$$

with constraints $u \in [0, 0.2722]$ and $V \leq 1.2$. The model equations are summarized in appendix A.

4.1 *Obtaining profit-to-go function*

The first step in simulation-based NDP optimization is to obtain a suboptimal profit-to-go function. This was done through simulations of a set of suboptimal heuristic policies. The heuristics were selected so that the 4-dimensional state space was sufficiently covered. The policies involved maintaining the reactor at initial volume $V(0)$ for certain amount of time t_i and then increasing the feed rate until end of fermentation time or until constraints are met (if V_{max} is reached before t_f, feed rate is reduced to $u = 0$ and reactor is operated in batch mode until $t = t_f$). Mathematically, the feed rate profiles followed were

$$u(t; t_i, b) = \begin{cases} 0 & \text{if } t < t_i \\ 0.02(1 + b(t - t_i)^{2.2}) & \text{if } t \geq t_i \end{cases}$$

We used four values of $b = [0.05, 0.07, 0.1, 0.13]$ and nine values of $t_i = [1, 2, \ldots, 9]$ to generate 36 different heuristic policies. Each of these policies were implemented for three different initial values of $V(0) = [0.4, 0.6, 0.8]$.

For each of the heuristic policies, the optimal ending time was determined — as the time that yielded the maximum profit value calculated according to Eq. (A.5). The productivity thus calculated gives the terminal reward function $\bar{\phi}_t = icV|_{t_f}$. Stage-wise reward is given by $\phi(x_k) = \lambda \Delta t_k$. Thus, for each of the states corresponding to a specific heuristic policy, the profit-to-go function is calculated as

$$J(x_k) = icV|_{t_f} - \lambda \cdot (t_f - t_k)$$

where $t_k = k.\Delta t$ is the "current" time for x_k.

We obtained a total of 9328 states and corresponding profit-to-go values through simulation of the heuristic policies. Next, a function approximator was used to correlate the profit-to-go as a function of system state. A backpropagation neural network was used that had 4 input nodes (corresponding to 4 state variables), 1 output node (profit-to-go) and two hidden layers with 17 and 5 nodes respectively. We denote this approximation as $\tilde{J}^0$.

Policy	Profit	$icV\|_{t_f}$	t_f
Patkar (1993)	3.70	7.30	12
Chaudhuri (1998)	3.50	7.10	12
Best heuristic	3.72	7.23	11.7
NDP	3.80	7.25	11.5

Table 1. Optimal control results for $V(0) = 0.6$.

Given this initial approximation of profit function, Bellman equation was used iteratively to improve the optimality of the profit-to-go approximation. For each of the 9328 data points, following equation was solved

$$\tilde{J}^{i+1} = \max \Big[icV|_{x_k} \max_{u_k} \Big\{ -\lambda \Delta t_k + \tilde{J}^i(x_{k+1}) \Big\} \Big]$$

Here, superscript i represents the iteration index. Δt represent time steps, which were taken to be constant and equal to 0.1 hours. Value iterations were performed as elaborated in section 3.1. Three iterations were required for the profit function to converge with 1-norm less than 0.2. The best neural network structures for each of the iterations were 4-17-5-1, 4-17-5-1 and 4-13-5-1 respectively.

Simulations using the converged profit-to-go approximator resulted in visits to regions of state space previously unvisited by heuristic controller. Hence, policy update was performed by including these unvisited states, and value iteration of Bellman equation was performed again. It took just one iteration for the profit function to converge. The neural network structure was found to be 4-15-5-1, and this $\tilde{J}^4$ was used for control.

5. RESULTS

The fourth trained neural network was implemented into online optimal control. The reactor was started with $V(0) = 0.6$. This was the case solved by Patkar *et al.* (1993) and Chaudhuri and Modak (1998). The results are shown in Table 1. State space plots for online controller performance are shown in Fig. 1. It can be seen from the figure that the optimal policy results from interpolation in the state space and not in the policy space.

The controller was then tested with different initial volume $V(0) = 0.5$. The results are shown in the second column in Table 2. This condition was not "seen" before by the function approximator. Next, we tested the controller in presence of unknown disturbance: abrupt cell death occurs at 9 h resulting in a 50% decrease in cell concentration. The NDP method still gives most optimal performance over the other methods. The best heuristic reported above is the heuristic that gave maximum profit value. It should be noted that

Policy	Profit $V_0 = 0.5$	Profit Cell death
Patkar *et al.* (1993)	3.74	0.62
Best heuristic	3.58	1.88
NDP	4.06	1.97

Table 2. Control results for a different V_0 and unknown disturbance cases

we found different heuristics to be the best for different $V(0)$ values. Thus, the optimal controller does not select any particular heuristic policy; instead it "patches" solution of various heuristics to come with a different, optimal policy.

6. CONCLUSIONS

A simulation-based Neuro-Dynamic Programming (NDP) strategy was applied to obtain optimal feeding profile for different initial conditions for invertase production in a fed-batch bioreactor. Simulation from suboptimal heuristic laws is used to identify relevant regions of the state space and to initialize the profit-to-go function approximation. The profit-to-go approximator is then improved by performing iterations of Bellman equation over only the relevant regions of the state space. The profit-to-go function thus obtained was then used for online optimal control. This method gives nearly optimal performance for different initial conditions without requiring to recompute the profit-to-go function. This method therefore has a promise in controlling fed-batch reactors in presence of disturbances.

7. REFERENCES

Banga, J. R., A. A. Alonso and R. P. Singh (1997). Stochastic dynamic optimization of batch and semicontinuous bioprocesses. *Biotechnology Progress* **13**, 326–335.

Bellman, R. E. (1957). *Dynamic Programming*. Princeton University Press. New Jersey.

Bertsekas, D. P. and J. N. Tsitsiklis (1996). *Neuro-Dynamic Programming*. Athena Scientific. Belmont, MA.

Bonvin, D., B. Srinivasan and D. Ruppen (2002). Dynamic optimization in the batch chemical industry. In: *Chemical Process Control–VI*. pp. 255–273.

Chaudhuri, B. and J. M. Modak (1998). Optimization of fed-batch bioreactor using neural network model. *Bioprocess Engineering* **19**, 71–79.

Cuthrell, J. E. and L. T. Biegler (1989). Simultaneous optimization and solution methods for batch reactor control profiles. *Computers and Chemical Engineering* **13**, 49–62.

Howard, R. (1960). *Dynamic programming and markov processes*. MIT Press. Cambridge Massachussets.

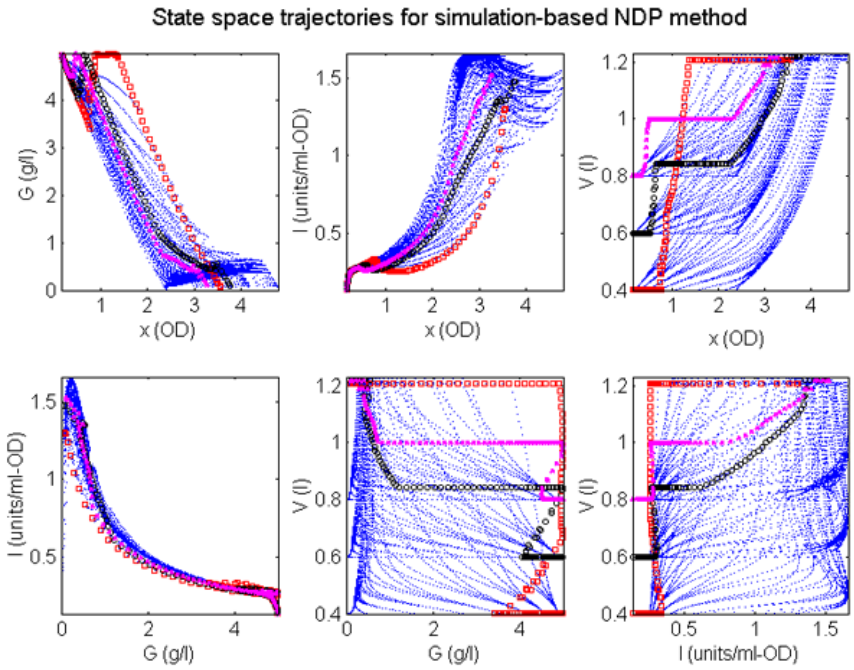

Fig. 1. State-space plot showing online performance for the three cases $V_0 = 0.4(\square)$, $V_0 = 0.6(\circ)$, and $V_0 = 0.8(\times)$. Dots represent the original data from heuristic feeding policies.

Kaisare, N. S., J. M. Lee and J. H. Lee (2002). Simultion based strategy for nonlinear optimal control: Application to a microbial cell reactor. Int. J. of Robust and Nonlinear Control, accepted for publication.

Lee, J. M. and J. H. Lee (2001). Neuro-dynamic programming method for mpc. In: *DYCOPS VI*. pp. 157–162.

Luus, R. (1993). Optimization of fed-batch fermentors by iterative dynamic programming. *Biotechnology and Bioengineering* **41**, 599–602.

Patkar, A. and J. H. Seo (1992). Fermentation kinetics of recombinant yeast in batch and fed-batch cultures. *Biotechnology and Bioengineering* **40**, 103–109.

Patkar, A., J. H. Seo and H. C. Lim (1993). Modeling and optimization of cloned invertase expression in *saccharomyces cerevisiae*. *Biotechnology and Bioengineering* **41**, 1066–1074.

Sutton, R. S. and A. G. Bartow (1998). *Reinforcement learning: an introduction*. MIT Press. Cambridge Massachussets.

Tsitsiklis, J. N. and B. Van Roy (1997). An analysis of temporal-difference learning with function approximation. *IEEE Transactions on Automatic Control* **42**, 674–690.

Watkins, C. J. C. H. and P. Dayan (1992). Q-learning. *Machine Learning* **8**, 279–292.

Appendix A. FED-BATCH REACTOR MODEL

Mass balance equations

$$(c\dot{V}) = (R_r Y_{cr} + R_f Y_{cf})\, cV \tag{A.1}$$

$$(s\dot{V}) = us_f - R_t cV \tag{A.2}$$

$$(i\dot{cV}) = (\pi - k_d i)\, cV \tag{A.3}$$

$$\dot{V} = u \tag{A.4}$$

where u is the feed rate, $c(OD)$, $s(g/L)$ and $i(units/OD/l)$ represent concentrations of cell, substrate and invertase respectively. The rate expressions are

$$R_r = \frac{0.55s}{0.05+s} \qquad R_t = \max\left\{\frac{1.25s}{0.95+s}, R_r\right\}$$

$$\pi = \frac{6.25s}{0.1+s+2s^2} \qquad R_f = R_t - R_r$$

$Y_{cr} = 0.6$, $Y_{cf} = 0.15$, $k_d = 1.85$.

Operating conditions: $c(0) = 0.15$, $s(0) = 5$, $i(0) = 0.1$, $s_f = 10$, $V(0) = \{0.4, 0.5, 0.6, 0.7, 0.8$.

Objective function:

$$\max_u \left\{ icV|_{t_f} - \lambda t_f \right\} \tag{A.5}$$

subject to constraints $0 \le u \le 0.2722$, $V \le 1.2$. Here, t_f is fermentation time, $\lambda = 0.3$ and sampling interval is $\Delta t = 0.1$.

GLUCOSE CONTROL IN TYPE I DIABETIC PATIENTS: A VOLTERRA MODEL–BASED APPROACH

Justin D. Rubb and Robert S. Parker

Department of Chemical and Petroleum Engineering
University of Pittsburgh
Pittsburgh, PA 15261 USA
rparker@pitt.edu

Abstract: Glucose concentration controllers for Type I diabetic patients are synthesized using model–based methods. A physiologically–based model of the insulin–dependent diabetic is employed as the patient. For modeling and control purposes, the patient is approximated using nonlinear Volterra series models. These data–driven models are then employed in two nonlinear controller synthesis strategies: internal model control using partitioned inverses (Doyle III *et al.*, 1995), and model predictive control.

Keywords: Biomedical systems, internal model control, model predictive control, nonlinear models, sampled-data systems, Volterra series

1. INTRODUCTION

In the normal patient, proper glucose control is maintained by the pancreatic β–cells; these cells alter their secretion of insulin, a potentiator for glucose removal from the bloodstream, in response to changing glucose levels. In the Type I (or insulin–dependent) diabetic patient, this control mechanism does not function properly, leading to sustained elevated blood glucose concentration and a condition known as hyperglycemia (defined as blood glucose $>$ 120 mg/dL). The Diabetes Complications and Control Trial (1993; 1996) has shown that this condition is responsible for many of the long–term effects of diabetes, such as blindness, kidney failure, and limb loss. While classical injection therapy can return the patient to near normoglycemic levels (glucose between 70 and 120 mg/dL), two primary drawbacks result from this treatment. First, the non–continuous nature of treatment often leads to wide variations in glucose concentration. In addition, over–delivery of insulin can result in significant drops in blood glucose concentration into the hypoglycemic range ($<$ 60 mg/dL). This low–glucose condition deprives the cells of fuel and can lead to coma and patient death. The maintenance of glucose within tight physiological limits is of supreme importance for the survival of diabetic patients.

The treatment of insulin–dependent diabetes currently employs insulin injection, inhalation delivery systems, or continuous infusion pumps. The inherent drawback of all of these approaches is their reliance on patient compliance to achieve long–term glucose control. The patient is normally required to adjust their insulin dose levels prior to meals, exercise, and sleep, and it is assumed that the patient delivers a correctly estimated dose at the proper time. The loss of glucose control may result from an incorrect estimate of insulin need or a missed dose. In an effort to remove the patient from the control loop, this work focuses on the development of a closed–loop insulin delivery system using periodic glucose measurements to calculate and deliver an insulin dose that will maintain the patient within the normoglycemic range in response to a variety of physiological disturbances.

Three primary components would compose a closed–loop insulin delivery system. Patient glucose measurements would be accomplished with an *in vivo* glucose concentration sensor; a significant effort is ongoing in this area (Jaremko and Rorstad, 1998). To

deliver variable amounts of insulin to the patient, there exist a variety of pump mechanisms (Cohen, 1993; Minimed Corporation, 1999). Linking the sensor and the delivery device is the control algorithm, on which this paper is focused. Classical feedback algorithms are inadequate for glucose control, due to the existence of system constraints and their interactions with the patient dynamics. The following work evaluates two candidate advanced control structures, nonlinear internal model control using partitioned model inverses (PNLI–IMC) and nonlinear model predictive control (NMPC), as well as their linear counterparts, with respect to their glucose control performance in response to glucose concentration challenges.

2. DIABETIC PATIENT CASE STUDY

The structure used as the diabetic patient in this work is the physiologically–based pharmacokinetic / pharmacodynamic model given in (Sorensen, 1985; Parker *et al.*, 2000). This model uses a compartmental technique to account for the connectivity and interaction of the various organs important to glucose and insulin metabolism and dynamics. From an input–output perspective, the steady state behavior is shown in Figure 1. In the local region of the nominal

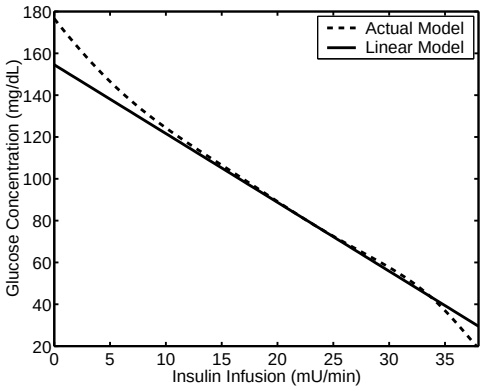

Fig. 1. Steady state locus for the diabetic patient. Nonlinear patient model (dashed), linear model (solid).

condition ($u_{ss} \approx 23.9$ mU/min, $y_{ss} \approx 81.1$ mg/dL), the diabetic patient displays linear behavior. However, more severe hypo– and hyperglycemic states elucidate the nonlinear character of the diabetic patient glucose–insulin response. The shape of the steady state locus motivates the use of polynomial empirical models to approximate the system behavior. Advantages of this approach include the relative ease with which empirical models can be identified and updated, as compared to more physiologically relevant models. Furthermore the calculation of the model inverse, for use in the control algorithm, can be facilitated by selecting certain model structures, as discussed in greater detail below (Doyle III *et al.*, 1995).

3. MODEL DEVELOPMENT

Model–based control systems require an accurate dynamic patient model. Given the significant variability observed in biomedical systems (Puckett and Lightfoot, 1995), an easily customizable model is preferable. These requirements lead to the use of empirical model structures for capturing patient dynamics. If a linear model is required, which facilitates controller synthesis, then discrete–time transfer functions can be employed. Alternatively, Volterra series, a member of the class of nonlinear moving average models, are effective in approximating nonlinear process dynamics (Boyd and Chua, 1985; Zheng and Zafiriou, 1994; Zheng and Zafiriou, 1995). Both structures are straightforward to update, and the decision about which model to employ depends on the control structure and desired performance.

3.1 *Volterra Series*

In an effort to capture the nonlinear characteristics of the diabetic patient, a nonlinear Volterra series model was selected to approximate the input–output behavior of the diabetic patient. Previous work (Florian and Parker, 2002) developed a Volterra model for the patient process described in Section 2. The remainder of this subsection will highlight those results as they form the basis for the model employed in the control studies.

The general Volterra series model has the form:

$$\hat{y}(k) = y_0 + \sum_{i=1}^{N} \sum_{j_1=1}^{M} \cdots \sum_{j_N=1}^{M} h_i(j_1, \ldots, j_N) \times u(k-j_1) \ldots u(k-j_N) \quad (1)$$

The diabetic patient can be approximated using the above discrete–time nonlinear model because the glucose–insulin dynamics display fading memory (Boyd and Chua, 1985); inputs further in the past have a lesser effect on the output than more recent input changes, up to a memory of M, beyond which the input effects are no longer significant. By selecting a model memory, M and model order, N, a truncated Volterra series can be employed to model a given system. Model coefficients ($h_i(j_1, \ldots, j_N)$) identified from patient data provide an empirical relationship (the Volterra model) between past insulin infusion rates ($u(k-i)$) and glucose concentration ($y(k)$) for a given patient at each sample time (k).

Starting from the general Volterra series model in equation (1), Florian and Parker (2002) showed that a third–order diagonal structure provides a good trade–off between identifiability (from limited clinical data) and predictive accuracy. The diagonal structure reduced the number of unknown model coefficients from 12,341 to 121, and decreased the

data requirements by orders of magnitude. This Volterra model can be decomposed as:

$$y(k) = h_0 + \mathscr{L}(k) + \mathscr{D}_2(k) + \mathscr{D}_3(k) \tag{2}$$
$$\mathscr{L}(k) = \sum_{i=1}^{M} h_1(i)u(k-i),$$
$$\mathscr{D}_2(k) = \sum_{i=1}^{M} h_2(i,i)u^2(k-i),$$
$$\mathscr{D}_3(k) = \sum_{i=1}^{M} h_3(i,i,i)u^3(k-i),$$

Here $\mathscr{L}$ denotes the linear terms, and diagonal terms of order N are given by $\mathscr{D}_N$. To facilitate the identification procedure, $y(k)$ and $u(k)$ are in scaled deviation form. In order to capture the dynamic response of the diabetic patient, the glucose sampling rate, T_s, and the model memory, M, were selected such that $\approx 99\%$ of the patient step response was captured by M coefficients, resulting in $T_s = 10$ min and $M = 40$. This is a reasonable memory length for application in controller synthesis, and the glucose sampling interval of 10 minutes is characteristic of current sensor development goals.

In model identification, tailored input sequences can dramatically reduce the amount of data necessary for model development while simultaneously offering improved coefficients (Parker *et al.*, 2001*a*). An input sequence of at least four discrete levels is required to identify a third–order Volterra model (Nowak and Van Veen, 1994). As in (Florian and Parker, 2002), a tailored five–level sequence was constructed that excited only the diagonal terms. The input sequence:

$$u(k) = \begin{cases} \gamma_1 & k = 0 \\ 0 & 1 \le k \le M \\ -\gamma_1 & k = M+1 \\ 0 & M+2 \le k \le 2M+1 \\ \gamma_2 & k = 2M+2 \\ 0 & 2M+3 \le k \le 3M+2 \\ -\gamma_2 & k = 3M+3 \\ 0 & 3M+4 \le k \le 4M+3 \end{cases} \tag{3}$$

is a special case of a continuous–switching–pace symmetric random sequence, where the sequence levels represent deviations from the nominal input value. In the previous identification study (Florian and Parker, 2002), it was established that $|\gamma_1| < |\gamma_2|$ provided superior estimates of model coefficients due to the lesser effect of the finite memory assumption for smaller inputs. Furthermore, the second–order diagonal coefficients were identified only from the γ_2 magnitude pulse responses, as these provided better stimulation of nonlinear behaviors. The sequence used to identify the Volterra model in equation (2) is shown in Figure 2

The identification objective was chosen to be minimization of model prediction error:

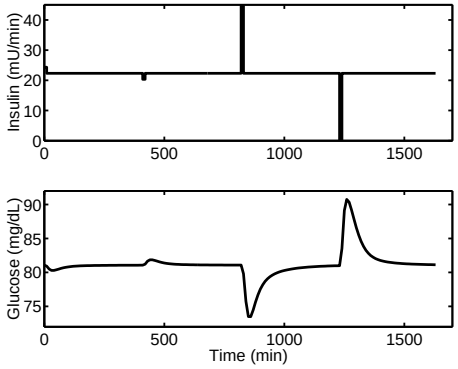

Fig. 2. Input sequence (top) and output response (bottom) for linear plus nonlinear diagonal coefficient identification.

$$J = \sum_{k=0}^{4M+3} e^2(k) = \sum_{k=0}^{4M+3} [y(k) - \hat{y}(k)] \tag{4}$$

In combination with the input sequence above, coefficient estimators can be analytically derived as in (Florian and Parker, 2002):

$$\hat{h}_0 = \frac{y(0)+y(M+1)}{4} + \frac{y(2M+2)+y(3M+3)}{4} \tag{5}$$

$$\hat{h}_1(k) = \frac{\gamma_2^3(y(k)-y(k+M+1))}{2\gamma_1\gamma_2(\gamma_2^2-\gamma_1^2)} - \frac{\gamma_1^3(y(k+2M+2)-y(k+3M+3))}{2\gamma_1\gamma_2(\gamma_2^2-\gamma_1^2)} \tag{6}$$

$$\hat{h}_2(k,k) = \frac{(y(k+2M+2)-y(2M+2))}{2\gamma_2^2} + \frac{(y(k+3M+3)-y(3M+3))}{2\gamma_2^2} \tag{7}$$

$$\hat{h}_3(k,k,k) = \frac{\gamma_2(y(k)-y(k+M+1))}{2\gamma_1\gamma_2(\gamma_2^2-\gamma_1^2)} - \frac{\gamma_1(y(k+2M+2)-y(k+3M+3))}{2\gamma_1\gamma_2(\gamma_2^2-\gamma_1^2)} \tag{8}$$

These estimators were updated from (Parker *et al.*, 2001*a*) to include third–order diagonal model estimation effects and the use of a partial sequence for second–order coefficient estimation. These estimators show superior performance in the absence of measurement noise; by repeating the input sequence in Figure 2, noise effects can be averaged over the number of repeats, as in (Parker *et al.*, 2001*a*).

4. CONTROLLER SYNTHESIS

While a significant amount of work has been performed in the area of controller synthesis for insulin–dependent diabetic patients (see (Parker *et al.*, 2001*b*) for a survey) the majority of these controllers employ linear patient models. The key

Table 1. Controller and model structure evaluation chart. The cells include the abbreviation used for the particular controller–model pairs.

		Controller	
		IMC	MPC
Model	Linear	LIMC	LMPC
	Nonlinear	PNLI-IMC	NMPC

contribution in the present study is the evaluation and comparison of two control structures, internal model control (IMC) using a partitioned model inverse and model predictive control (MPC), when the models employed are clinically–relevant empirical models of the Volterra type. Table 1 provides the abbreviations used for the controllers under evaluation. In all cases, the controllers were designed to accommodate a sampling rate of 1 measurement per 10 min. Based on current sensor research (Jaremko and Rorstad, 1998), this sampling rate provides a reasonable trade–off between the capabilities of sensing technology and the controller performance needs.

4.1 *IMC Synthesis*

Synthesis of a linear discrete–time IMC controller can be accomplished using a variety of techniques (discretization of a continuous–time controller, discrete–time synthesis, etc.) (Ogunnaike *et al.*, 1994). In the present work, a discrete–time transfer–function model ($G(z)$) was constructed to approximate the linear Volterra series model. By appending a first–order filter (time constant ϕ) to the linear inverse, the discrete–time IMC controller was synthesized. The resulting transfer function model and LIMC controller were:

$$G(z) = \frac{-0.458}{z - 0.849} \tag{9}$$

$$Q(z) = \frac{(1-\phi)z - 0.849(1-\phi)}{-0.458z + 0.458\phi} \tag{10}$$

The quality of model fit can be seen in Figure 3.

Partitioned nonlinear inverse controller synthesis was accomplished using the approach of Doyle III *et al.* (1995), in discrete–time with the third–order diagonal Volterra model. If the linear inverse exists, then a nonlinear system $\mathscr{P}$ that can be partitioned as

$$\mathscr{P} = (\mathscr{L} + \mathscr{N}) = \mathscr{L}(\mathscr{I} + \mathscr{L}^{-1}\mathscr{N})$$

can be analytically inverted yielding:

$$\mathscr{P}^{-1} = (\mathscr{I} + \mathscr{L}^{-1}\mathscr{N})^{-1}\mathscr{L}^{-1}$$

In block diagram form, this can be constructed as shown in Figure 4. Here the linear controller ($\mathscr{L}^{-1}$) is the transfer function in Equation (9), written in difference equation form. The nonlinear controller component ($\mathscr{N}$) is comprised of the $\mathscr{D}_2$ and $\mathscr{D}_3$

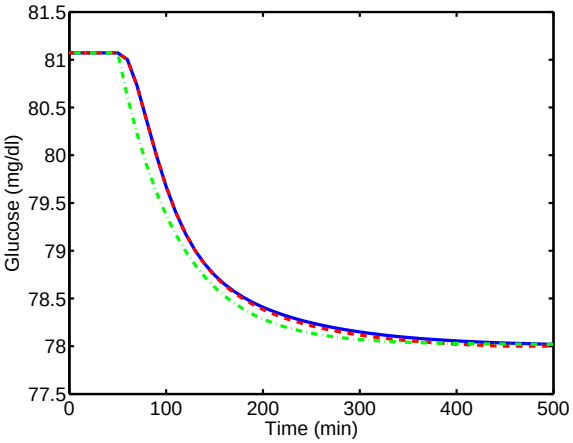

Fig. 3. Comparison of model dynamics. Solid: actual patient (continuous); dashed: linear Volterra; dash–dot: transfer function.

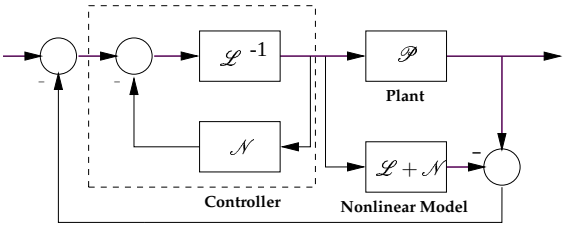

Fig. 4. PNLI–IMC schematic

components of the Volterra model (2). The difference equation formulation facilitates the "while" loop structure required for the controller loop to converge, an effect of the direct–feed nature of the controller and the static nonlinearities in the feedback loop. The convergence criterion is a difference in consecutive insulin infusion rate calculations of 1×10^{-4} mU/min.

The IMC controller (in both linear and PNLI–nonlinear forms) contains a single tuning parameter: the filter time constant. Since the controller is designed primarily to reject meal disturbances from a pseudo–steady state, the value of the filter constant could be selected to be small (in this case $\phi = 0.1$) to allow aggressive disturbance rejection. Should setpoint changes become a concern, or if sharp discontinuities were to occur in the measurement signal, the controller would have to be detuned significantly (to approximately $\phi = 0.7$) to maintain stability.

4.2 *MPC Synthesis*

Model predictive control is an algorithm that employs a process model to predict future dynamic behavior based on past inputs. This is an optimization–based control algorithm, executing at each sample time, and it uses the following objective function:

$$\min_{\Delta\mathscr{U}(k|k)} \|\Gamma_y[\mathscr{R}(k+1) - \mathscr{Y}(k+1|k)]\|_2^2 + \|\Gamma_u \Delta\mathscr{U}(k|k)\|_2^2 \tag{11}$$

Over a future prediction horizon of p steps, a series of $m \leq p$ manipulated variable moves is calculated in order to minimize the objective in Equation (11). The matrices Γ_y and Γ_u are used to trade off setpoint tracking error and manipulated variable movement, respectively. Additional constraints on the manipulated and controlled variables can be implemented in a straightforward fashion, as this is an optimization problem. In the case of a linear process model, the resulting problem is a quadratic programming problem. This changes to a nonlinear programming problems when nonlinear process models are employed. To solve the quadratic and nonlinear programming problems, the *fmincon* optimization routine of MATLAB (©2002, The Mathworks, Natick, MA) was employed.

Selecting the tuning parameters for a model predictive control algorithm is typically done on an *ad hoc* basis; there is no optimal tuning algorithm available. In general, the move and prediction horizons are adjusted to provide sufficient aggressiveness in control action, as well as adequate model prediction. The tuning matrices are used to alter the setpoint tracking performance (Γ_y) and to suppress noise–induced manipulated variable adjustment (Γ_u).

4.3 *Results and Discussion*

The results of using nonlinear compensation within the IMC framework to reject a meal disturbance of 50 grams (glucose) at time $t = 50$ min can be seen in Figure 5. A slightly more aggressive controller

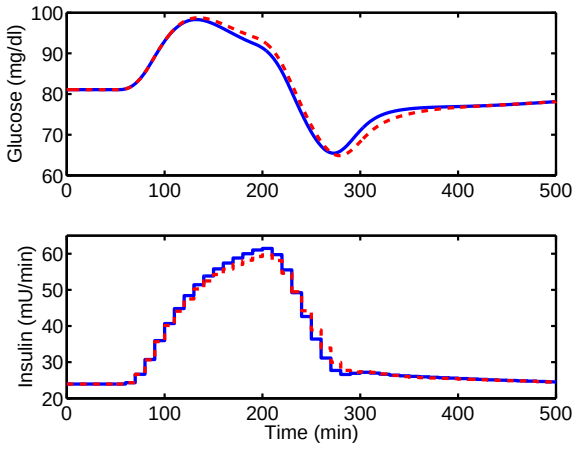

Fig. 5. 50 g meal disturbance simulation comparing LIMC (dashed) and PNLI–IMC (solid). The filter time constant was selected as $\phi = 0.1$ in both cases.

results from using the PNLI–IMC framework, as the nonlinear controller both increases and decreases the insulin delivery rate more rapidly than the linear controller. The sum–squared error (SSE) was reduced by 6.5%, with a small (3.7%) improvement in glucose concentration undershoot to a minimum of 65.5 mg/dl. Simulation results evaluating the model predictive control algorithm for the same disturbance as above are shown in Figure 6. The increased aggressiveness

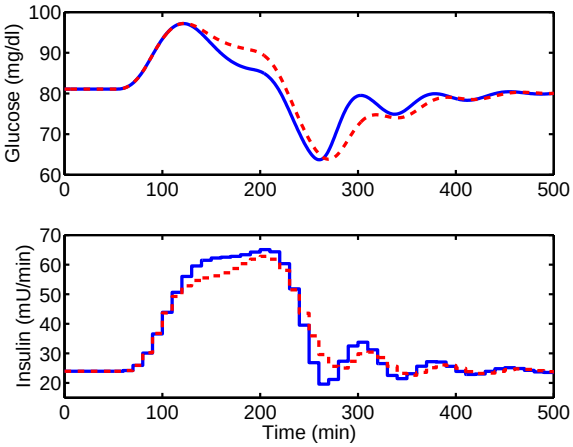

Fig. 6. 50 g meal disturbance simulation comparing MPC (dashed) and NMPC (solid). The tuning parameters for both controllers were $\Gamma_y = 3$, $\Gamma_u = 1$, $m = 3$, $p = 8$.

of the nonlinear controller can be clearly observed in the manipulated variable profile, where the insulin delivery rate is elevated more quickly and to a higher maximum delivery rate. This leads to the glucose concentration decrease observed between $t = 150$ and $t = 200$ min. Furthermore, the nonlinear controller decreases its delivery rate more quickly, thereby compensating more efficiently for the hypoglycemic excursion around $t = 270$ min. For an 0.3% increase in total insulin delivery, the nonlinear controller provides a 13% decrease in sum–squared error and a more rapid reaction to hypoglycemic excursions.

The increased ability to tailor the performance objective in MPC leads to a marked increase in performance as defined by sum–squared error, as shown in Table 2. This improvement in error is a

Table 2. Controller performance comparison. Absolute (mg^2/dl^2) and comparative (%) metrics versus linear IMC shown.

	Linear		Nonlinear	
	SSE	%	SSE	%
IMC	213	0	199	6.5
MPC	187	12	163	23.3

result of decreasing the magnitude and duration of the hyperglycemic excursion (between $t = 100$ and $t = 200$), as well as the return to steady state after the hypoglycemic excursion. The NMPC algorithm is particularly responsive to the depressed glucose concentrations between $t = 220$ and $t = 270$ min, and its aggressive response leads to superior performance. The fact that this nonlinear control algorithm responds so aggressively to the hypoglycemic excursion is imperative for diabetic patients in whom dramatically suppressed glucose levels can lead to coma and death. One minor penalty for improving the SSE is increased

undershoot. Both MPC controllers lead to minimum glucose concentrations of about 2 mg/dl less than the IMC controllers. However, the difference is well within the noise band of present sensors.

5. CONCLUSIONS

This paper presents an analysis of linear and nonlinear model–based control algorithms as employed in simulation on insulin–dependent diabetic patients. By employing a previously–developed parsimonious nonlinear Volterra series model (Florian and Parker, 2002) in the control structure, nonlinear control algorithms (IMC with partitioned inverses and MPC) were synthesized. These algorithms were then tested with respect to their capabilities in meal disturbance rejection. Nonlinear compensation proved beneficial, especially as the patient deviated from the nominal condition of 81 mg/dl. Given the performance metric of SSE, the NMPC controller is superior; however, if constraints are not imposed and a closed–form controller solution is required then linear MPC would be the best choice. In all cases, the utility of empirical model structures identified from patient data have proven effective in controlling glucose concentration in the presence of meal disturbances.

6. ACKNOWLEDGMENTS

The authors would like to acknowledge partial funding for this work from the Fulton C. Noss Faculty Fellowship of the University of Pittsburgh and the Pittsburgh Tissue Engineering Initiative.

7. REFERENCES

Boyd, S. and L. O. Chua (1985). Fading memory and the problem of approximating nonlinear operators with Volterra series. *IEEE Trans. Cir. Sys.* **CAS-32**(11), 1150–1161.

Cohen, A. (1993). New disposable electronic micropump for parenteral drug delivery. In: *Pulsatile Drug Delivery: Current Applications and Future Trends* (R. Gurny, H.E. Junginger and N.A. Peppas, Eds.). pp. 151–161. Wissenschaftliche, Stuttgart.

DCCT - The Diabetes Control and Complications Trial Research Group (1993). The effect of intensive treatment of diabetes on the development and progression of long–term complications in insulin–dependent diabetes mellitus. *N. Engl. J. Med.* **329**, 977–986.

DCCT - The Diabetes Control and Complications Trial Research Group (1996). The absence of a glycemic threshold for the development of long–term complications: The perspective of the diabetes control and complications trial. *Diabetes* **45**, 1289–1298.

Doyle III, F. J., B. A. Ogunnaike and R. K. Pearson (1995). Nonlinear model-based control using second-order Volterra models. *Automatica* **31**, 697–714.

Florian, J. A. and R. S. Parker (2002). A nonlinear data–driven approach to type I diabetic patient modeling. 15th IFAC World Congress on Automatic Control. IFAC.

Jaremko, J. and O. Rorstad (1998). Advances toward the implantable artificial pancreas for treatment of diabetes. *Diabetes Care* **21**, 444–450.

Minimed Corporation (1999). The minimed 507c, products and specifications. URL: http://www.minimed.com/files/mm_098.htm.

Nowak, R. D. and B. D. Van Veen (1994). Random and pseudorandom inputs for Volterra filter identification. *IEEE Trans. Signal Processing* **42**(8), 2124–2135.

Ogunnaike, B. A., R. K. Pearson, N. Samardzija and J. D. Bomberger (1994). Low order emprical modeling for nonlinear systems. In: *IFAC Symposium on Advanced Control of Chemical Processes*. Kyoto, Japan. pp. 41–46.

Parker, R. S., D. Heemstra, F. J. Doyle III, R. K. Pearson and B. A. Ogunnaike (2001*a*). The identification of nonlinear models for process control using tailored "plant–friendly" input sequences. *J. Proc. Control* **11, Sp. Issue SI**, 237–250.

Parker, R. S., F. J. Doyle III and N. A. Peppas (2001*b*). The intravenous route to blood glucose control. *IEEE Eng. Med. Biol.* **20**, 65–73.

Parker, R. S., J. H. Ward, N. A. Peppas and F. J. Doyle III (2000). Robust H_∞ glucose control in diabetes using a physiological model. *AIChE Journal* **46**, 2537–2549.

Puckett, W.R. and E.N. Lightfoot (1995). A model for multiple subcutaneous insulin injections developed from individual diabetic patient data. *Am. J. Physiol* **269 (Endocrinol. Metab. 32)**, E1115–E1124.

Sorensen, J.T. (1985). A Physiologic Model of Glucose Metabolism in Man and its Use to Design and Assess Improved Insulin Therapies for Diabetes. PhD thesis. Department of Chemical Engineering, MIT.

Zheng, Q. and E. Zafiriou (1994). Control-relevant identification of Volterra series models. In: *Proc. American Control Conf.*. Baltimore, MD. pp. 2050–2054.

Zheng, Q. and E. Zafiriou (1995). Nonlinear system identification for control using Volterra-Laguerre expansion. In: *Proc. American Control Conf.*. Seattle, WA. pp. 2195–2199.

BIOMASS RECONSTRUCTION IN A WASTEWATER TREATMENT BIOFILTER

A. Vande Wouwer[*1], C. Renotte[*], N. Deconinck[+], Ph. Bogaerts[+]

[*]*Laboratoire d'Automatique, Faculté Polytechnique de Mons, 31 Boulevard Dolez, 7000 Mons, Belgium*
([1]tel: +32-(0)65-374141; fax: +32-(0)65-374136;
email: Alain.VandeWouwer@fpms.ac.be)
[+]*Service d'Automatique, Université Libre de Bruxelles, Brussels, Belgium*

Abstract: this paper is concerned with a pilot-scale fixed-bed biofilter used for nitrogen removal from municipal wastewater. Process dynamics is described by a set of mass balance partial differential equations, which allow the evolution of the several component concentrations along the biofilter axis to be reproduced. Based on sets of experimental data collected over a several-month period, unknown model parameters are estimated by minimizing an output error criterion. The resulting distributed parameter model and a few pointwise measurements of nitrate, nitrite, and ethanol concentrations can be used to design observers, which allow the unmeasured biomass concentrations to be reconstructed on-line. First, it is demonstrated that asymptotic observers are unsuitable for the model structure. Then, a receding-horizon observer is designed and tested, which shows very satisfactory performance.

Keywords – distributed parameter systems, state estimation, identification, biotechnology.

1. INTRODUCTION

Nitrogen removal is an important step in the treatment of municipal wastewater. Over the past several years, biofilter systems have received considerable attention; see for instance the conference proceedings and journals of the International Water Association (IWA) (e.g. Oh *et al.*, 2001). The main advantages of these wastewater treatment systems are their ease of use, compactness, efficiency, and low energy consumption.

In a previous study (Vande Wouwer et al., 2002), a dynamic model was developed based on experimental data collected from a pilot-scale plant. The resulting model can be used for simulation purposes (e.g. for system analysis and design) or as a basis for the development of a software sensor (which can be used to estimate unmeasured variables on-line). In contrast to a similar study by Bourrel et al. (1996; 2000), the proposed model does not assume that steady state biomass conditions are achieved, but on the opposite explains the very long transient phases observed experimentally by growth and inactivation processes associated to the biomass.

The biomass distribution inside the biofilter therefore appears as a primary determinant of the plant performance. Based on a few pointwise measurements of nitrate, nitrite and ethanol concentrations, and on the biofilter model, the objective of this paper is to design distributed parameter observers of the unmeasured biomass concentration profiles. Asymptotic observers (Bastin and Dochain, 1990), which do not rely on the knowledge of the kinetic model and which have good convergence properties in the case of continuous systems, would a priori be a very appealing solution. However, they appear unsuitable for the model structure, and attention is therefore focused on

receding-horizon observers (Allgöwer et al., 1999; Bogaerts and Hanus, 2001), which allow the state estimation problem for nonlinear distributed parameter systems to be solved in a very elegant way.

This paper is organized as follows. In the next section, the experimental setup is described. Section 3 briefly discusses biofilter modeling, i.e. the derivation of a reaction scheme, reaction kinetics, and a system of mass balance PDEs. In Section 4, distributed parameter asymptotic observers and receding-horizon observers for the unmeasured biomass concentration profiles are examined. Finally, Section 5 is devoted to some conclusions.

2. PROCESS DESCRIPTION

The pilot plant under consideration (Fig. 1) is a submerged biofilter packed with lava rock (pouzzolane). The biofilter is fed with a synthesis water composed of raw municipal wastewater and additions of a concentrated nitrate solution. Several biological reactions take place inside the biofilter, e.g. removal of soluble COD and removal of nitrate and nitrite.

The denitrification process consists of several consecutive reactions of oxydo-reduction and implies a transient accumulation of nitrite in the biofilter

$$NO_3^- \xrightarrow{(1)} NO_2^- \xrightarrow{(2)} N_2$$

Oxydo-reduction is achieved thanks to an organic carbon source (as donor of electrons). In this case, ethanol is used.

Eight sampling points are evenly distributed along the reactor axis, which allow the several component concentration profiles (COD, nitrate and nitrite) to be measured. The manipulated variables are the feed flow rate F(t) to the biofilter and the inlet ethanol concentration $S_{C,in}(t)$.

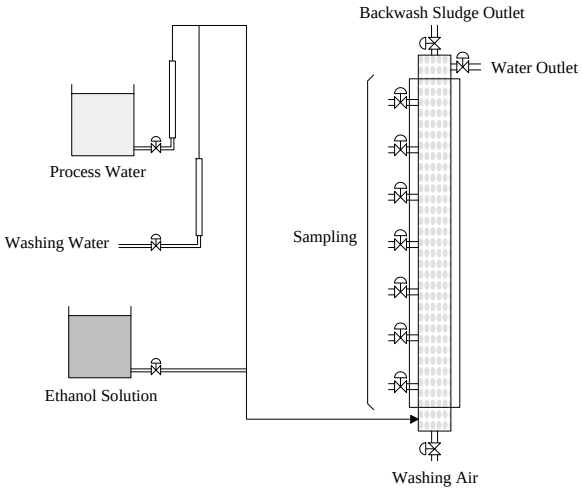

Fig. 1. Experimental setup

The experiments accomplished with the pilot plant aimed at sweeping the range of operating conditions (various C/N and feed-flow rates; on the other hand, the temperature was kept constant) observed in a full-scale wastewater treatment plant located in Montargis, France. The experiments were carried out at the Institut National des Sciences Appliquées de Toulouse (INSAT), France (Bascoul, 1995).

3. MODEL DEVELOPMENT

In this section, a system of mass-balance PDEs is derived, and the unknown model parameters are estimated from experimental data (for more details see (Vande Wouwer et al., 2002)).

3.1 Reaction scheme

A macroscopic biological reaction scheme based on the concept of "pseudo-stoichiometry" (Bastin and Dochain, 1990) is used

$$\nu_1 \text{carbon} + \frac{\nu_2}{\alpha_1}\text{nitrate} \rightarrow \text{biomass} + \frac{\nu_2}{\alpha_2}\text{nitrite} \quad (1)$$

$$\nu_3 \text{carbon} + \frac{\nu_4}{\alpha_2}\text{nitrite} \rightarrow \text{biomass} + \nu_5 \text{nitrogen} \quad (2)$$

$$\text{active biomass} \rightarrow \text{inactive biomass} \quad (3)$$

where ν_i , i = 1,…,5 are the pseudo-stoichiometric coefficients, and α_1 = 1.14, α_2 = 1.71 are Chemical Oxygen Demand (COD) conversion factors.

3.2. Reaction kinetics

The specific growth rates are taken in the form

$$\mu_1 = \mu_{1,\max} \frac{S_{NO3}}{S_{NO3} + K_{NO3}} \frac{1}{1 + X_a / K_{Xa1}} \quad (4)$$

$$\mu_2 = \mu_{2,\max} \frac{S_{NO2}}{S_{NO2} + K_{NO2}} \frac{1}{1 + X_a / K_{Xa2}} \quad (5)$$

$$\mu_3 = \mu_{3,\max} \quad (6)$$

where the limiting substrates are nitrate (S_{NO3}) and nitrite (S_{NO2}). The active biomass X_a has an inhibition effect on the two growth-associated reactions (1-2). The inactivation process is assumed to have first-order kinetics (the simplest possible model in the absence of detailed knowledge about this process). In the experiments considered in this study, the carbon source is always in excess so that its limiting effect cannot be quantified.

3.3. Mass balances

Based on this reaction scheme and kinetics, it is straightforward to derive the following mass balance PDEs

$$\frac{\partial S_{NO3}}{\partial t} = -v\frac{\partial S_{NO3}}{\partial z} - \frac{\nu_2'}{\alpha_1}\mu_1 X_a \quad (7)$$

$$\frac{\partial S_{NO2}}{\partial t} = -v\frac{\partial S_{NO2}}{\partial z} + \left(\frac{\nu_2'}{\alpha_2}\mu_1 - \frac{\nu_4'}{\alpha_2}\mu_2\right)X_a \quad (8)$$

$$\frac{\partial S_C}{\partial t} = -v\frac{\partial S_C}{\partial z} - \left(\nu_1'\mu_1 - \nu_3'\mu_2\right)X_a \quad (9)$$

$$\frac{\partial X_a}{\partial t} = \left(\mu_1 + \mu_2 - \mu_3\right)X_a \quad (10)$$

where plug-flow conditions are assumed, $v = \frac{F}{\varepsilon A}$ is the fluid flow velocity (A: cross-section area of the biofilter, ε : bed porosity), and $\nu_i' = \frac{1-\varepsilon}{\varepsilon}\nu_i$.

These equations are supplemented by boundary conditions corresponding to the inlet concentrations.

PDEs (7-10) are solved numerically using a standard method of lines procedure (finite differences with about 30 nodes).

3.4. Parameter estimation

Pseudo-stoichiometry and kinetics involve 11 unknown model parameters (ν_i , i = 1,..,4, $\mu_{i,max}$, i = 1,..,3, K_{NO3}, K_{NO2}, K_{Xa1} and K_{Xa2}), whose numerical values have to be inferred from experimental data.

Based on the assumption of constant (but unknown) relative errors on the measurement data, the following output-error criterion is defined:

$$J = \sum_{k=1}^{15}\sum_{i=1}^{3}\sum_{l=1}^{8}\left(\ln(y_{i,mes}(z_l,t_k)) - \ln(y_{i,mod}(z_l,t_k))\right)^2 \quad (11)$$

where:

- constant relative errors on the measurements $y_{i,mes}$ are equivalent to constant absolute errors on the logarithms of the measurements $\ln(y_{i,mes})$,
- 15 sample times, at each of which 3 component concentrations (S_C, S_{NO3} and S_{NO2}) in 8 different spatial locations are measured, representing a total of 360 data points.

The output-error criterion (11) is minimized with respect to the unknown model parameters using a Levenberg-Marquardt algorithm. Positivity constraints on the parameters are imposed through a logarithmic transformation.

The model prediction is compared to the measured signals (direct and cross-validation); see for instance Fig. 2, which shows the spatial concentration profile of nitrite, at a particular sample time. The model agreement is satisfactory.

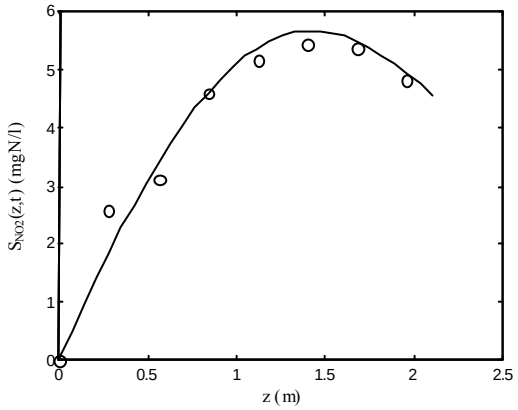

Fig. 2: Spatial nitrite concentration profile (direct validation - solid line: model prediction, circles: measured values).

4. STATE ESTIMATION

The long transient phases observed in real-life operations can be explained by biomass growth and inactivation processes, i.e. the global rate at which biomass develops determines the overall dynamics of the biofilter. The uniformity of the biomass distribution inside the porous bed is also a primary determinant of the biofilter performance in face of large variations of the feed conditions. For process monitoring, it would therefore be interesting to visualize the biomass concentration profiles on-line. However, these profiles are difficult to measure in practice, and it is required to resort to state estimation techniques. With regard to the modeling uncertainties, particularly of the reaction kinetics, it is appealing to design an asymptotic observer (Bastin and Dochain, 1990), which is the first solution considered in the following.

4.1. Asymptotic observers

The mass balance PDEs (7-10) can be reformulated in a more compact form as follows

$$\frac{\partial \boldsymbol{\xi}}{\partial t} = -\mathbf{v}\frac{\partial \boldsymbol{\xi}}{\partial z} + \mathbf{K}\boldsymbol{\varphi} \quad (12)$$

or

$$\frac{\partial}{\partial t}\begin{bmatrix}\boldsymbol{\xi}_f \\ \boldsymbol{\xi}_s\end{bmatrix} = \begin{bmatrix}-v\cdot\dfrac{\partial \boldsymbol{\xi}_f}{\partial z} \\ 0\end{bmatrix} + \begin{bmatrix}\mathbf{K}_f \\ \mathbf{K}_s\end{bmatrix}\cdot\boldsymbol{\varphi} \quad (13)$$

where $\mathbf{v}$ is the velocity vector, $\mathbf{K}$ is the pseudo-stoichiometry matrix, $\boldsymbol{\varphi} = \boldsymbol{\mu}X_a$ is the reaction rate vector, and the state $\boldsymbol{\xi} = [S_{NO3} \quad S_{NO2} \quad S_C \quad X_a]^T$ is decomposed into the components in solution in the

fluid phase $\xi_f = [S_{NO3} \quad S_{NO2} \quad S_C]^T$, which can be measured on-line in a few locations along the reactor axis, and the component anchored on the solid phase $\xi_s = [X_a]$, which is not measured.

Following (Bastin and Dochain, 1990; Dochain and Vanrolleghem, 2001), the procedure to develop an asymptotic observer is to partition ξ into two subvectors ξ_a and ξ_b, $\xi = [\xi_a \quad \xi_b]^T$, such that the corresponding partition of the pseudo-stoichiometry matrix $\mathbf{K} = [\mathbf{K}_a \quad \mathbf{K}_b]^T$ with

$$\mathbf{K} = \begin{bmatrix} -\nu_2/\alpha_1 & 0 & 0 \\ \nu_2/\alpha_2 & -\nu_4/\alpha_2 & 0 \\ -\nu_1 & -\nu_3 & 0 \\ 1 & 1 & -1 \end{bmatrix} \tag{14}$$

is of full row rank. Here, rank (**K**) = M = 3 (M is the number of independent reactions in the reaction scheme), so that rank ($\mathbf{K}_a$) should be 3.

This condition excludes the commonly used partition into measured and non measured components, i.e. $\xi_a = \xi_f$ and $\xi_b = \xi_s$, as rank ($\mathbf{K}_a$) = 2 only. Hence, the following partition is selected

$$\xi_a = \begin{bmatrix} \xi_{af} \\ \xi_{as} \end{bmatrix} = \begin{bmatrix} S_{NO_3} \\ S_{NO_2} \\ X_a \end{bmatrix} \quad \text{and} \quad \xi_b = [S_C] \tag{15}$$

which leads to a full row rank submatrix $\mathbf{K}_a$.

It is then possible to define a new state vector **z** by

$$\mathbf{z} = \mathbf{A}_0 \xi_a + \xi_b = [\mathbf{A}_{0f} \quad \mathbf{A}_{0s}] \begin{bmatrix} \xi_{af} \\ \xi_{as} \end{bmatrix} + \xi_b \tag{16}$$

where the matrix $\mathbf{A}_0$ is the unique solution of

$$\mathbf{A}_0 \mathbf{K}_a + \mathbf{K}_b = 0 \tag{17}$$

The evolution of **z** is given by

$$\frac{\partial \mathbf{z}}{\partial t} = \mathbf{A}_{0f} \cdot \frac{\partial \xi_{af}}{\partial t} + \mathbf{A}_{0s} \cdot \frac{\partial \xi_{as}}{\partial t} + \frac{\partial \xi_b}{\partial t} \tag{18}$$

Substituting the time derivatives by their expressions (13), the equations of the asymptotic observer, from which the reaction kinetics are eliminated, are obtained

$$\frac{\partial \hat{\mathbf{z}}}{\partial t} = -v \cdot \left(\mathbf{A}_{0f} \cdot \frac{\partial \xi_{af}}{\partial z} + \frac{\partial \xi_b}{\partial z} \right) \tag{19}$$

$$\hat{\xi}_{as} = \mathbf{A}_{0s}^{-1} \cdot \left(\hat{\mathbf{z}} - \mathbf{A}_{0f} \cdot \xi_{af} - \xi_b \right) \tag{20}$$

For this observer to be completely defined, the inverse $\mathbf{A}_{0s}^{-1}$ (which, in the particular case under consideration, is a scalar) is required. This information can be obtained by solving equation (17), which gives $\mathbf{A}_{0s} = 0$!

The asymptotic observer is therefore not applicable with the model structure (13) since the partition of the state vector leads either to a submatrix $\mathbf{K}_a$ which is not full row rank or to a null matrix $\mathbf{A}_{0s}$. The only way round would be to simplify the model and to abandon the equation describing the biomass inactivation process (as was the case in the work of Bourrel *et al.*, 2000), which we know is not acceptable.

4.2. Receding-horizon observers

As the concentration measurements are rare and corrupted by noises, the concept of full-horizon observer (Bogaerts and Hanus, 2001), which uses all the measurement information available up to the current time, is extended to the distributed parameter model of the biofilter.

The *prediction step* (between samples $t_k < t < t_{k+1}$) corresponds to the solution of the model PDEs (12)

$$\frac{\partial \hat{\xi}}{\partial t} = -\mathbf{v} \frac{\partial \hat{\xi}}{\partial z} + \mathbf{K}\boldsymbol{\varphi}(\hat{\xi}) \qquad 0 \le t < t_{k+1} \tag{21}$$

subject to initial conditions

$$\hat{\xi}(0) = \hat{\xi}_{0/k} \tag{22}$$

and boundary conditions corresponding to the inlet concentrations.

The *correction step* (at sampling times) corresponds to the following optimization problem:

$$\hat{\xi}_{0/k} = \underset{\xi_0}{\text{Arg min}}\, J_k(\xi_0) \tag{23}$$

with $J_k(\xi_0)$ given by

$$\frac{1}{2} \sum_{j=1}^{k} (\mathbf{y}_{mes}(t_j) - \mathbf{y}_{mod}(t_j))^T \mathbf{Q}(t_j)^{-1} (\mathbf{y}_{mes}(t_j) - \mathbf{y}_{mod}(t_j)) \tag{24}$$

$$J_k(\xi_0) = \frac{1}{2} \sum_{j=1}^{k} (\mathbf{y}_{mes}(t_j) - \mathbf{y}_{mod}(t_j))^T \mathbf{Q}(t_j)^{-1} (\mathbf{y}_{mes}(t_j) - \mathbf{y}_{mod}(t_j))$$

where $\mathbf{y}_{mes}$ represents the vector of measurements (nitrate, nitrite and ethanol concentrations in 8 locations along the biofilter axis), $\mathbf{y}_{mod}$ the

corresponding model prediction, and **Q** the covariance matrix of the measurement errors.

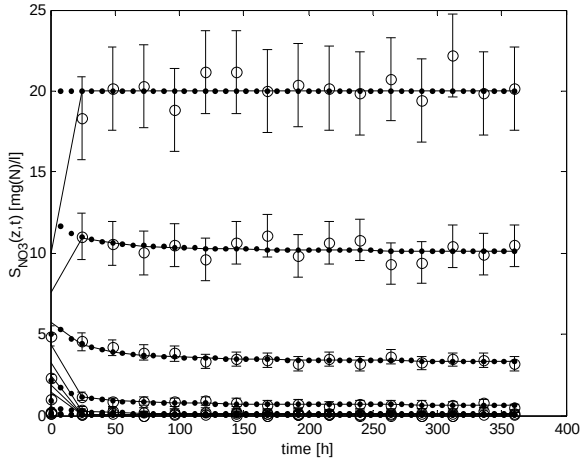

Fig. 3: Temporal evolution of the real (dots) and estimated (solid lines) nitrate concentrations in the 8 measurement locations, and concentration measurements (circles) together with their 99% confidence intervals.

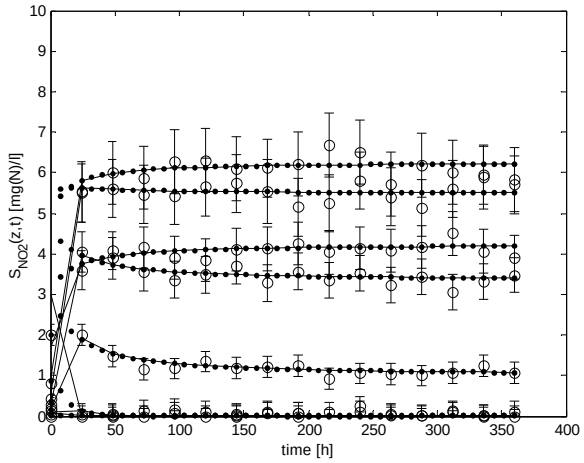

Fig. 4: Temporal evolution of the real (dots) and estimated (solid lines) nitrite concentrations in the 8 measurement locations, and concentration measurements (circles) together with their 99% confidence intervals.

In order to reduce the dimensionality of the optimization problem (27-28), the vector of initial conditions $\hat{\xi}_{0/k}$ is expressed as a set of exponential profiles, i.e.

$$\hat{\xi}_{0,i}(z) = \alpha_i \cdot \exp(-\beta_i \cdot z) \qquad (25)$$

($i = S_{ON3}$, S_{ON2}, S_C, X_a) which leads to the on-line determination of 8 parameters.

The observer is first tested in simulation. The biofilter model is used to generate simulation data, which are corrupted by noise. Figures (3-4) compare the temporal evolution of the real and estimated concentrations in the 8 measurement locations distributed along the biofilter axis, as well as the measured concentrations together with their 99% confidence intervals. Figure (5) compares the biomass estimates with their real values (which are not measured), whereas figure (6) illustrates the time evolution of the corresponding spatial profiles.

As it is apparent from figures (3-6), the performance of the full-horizon observer is very satisfactory. Experimental application confirms this observation, as depicted in figures (7-8) which show the initial nitrite concentration profiles (initial measured profile and initial exponential guess) and the same profiles after 404 hours. The convergence of the observer is satisfactory, despite the modeling errors and the measurement noise. The observer performance cannot however be fully tested, as biomass measurements are not available.

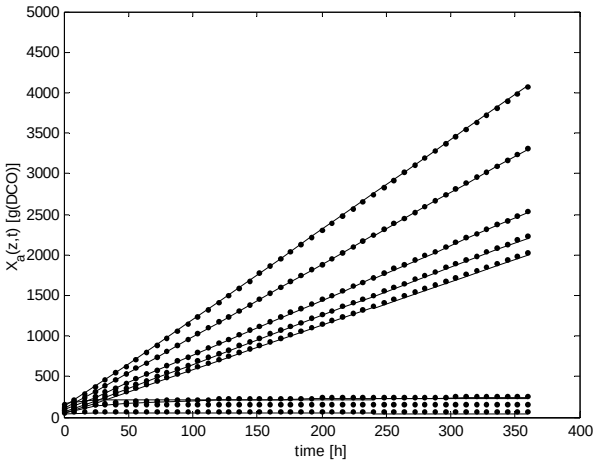

Fig. 5: Temporal evolution of the biomass concentration estimates (solid lines) and of the real, non measured, concentrations (dots).

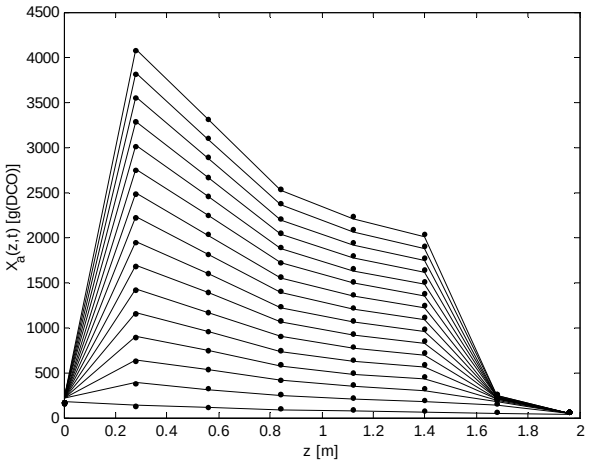

Fig. 6: Temporal evolution of the biomass spatial profiles (solid lines) and of the real, non measured, concentrations (dots).

5. CONCLUSION

In this paper, a distributed parameter model of a

fixed-bed biofilter used for nitrogen removal in municipal wastewater treatment is derived. The unknown model parameters are estimated from experimental data collected over a period of several months. The main contribution of this modeling study is to show that the long transient phases observed in real-life operations can be explained by biomass growth and inactivation processes, i.e. the global rate at which biomass develops determines the overall dynamics of the biofilter.

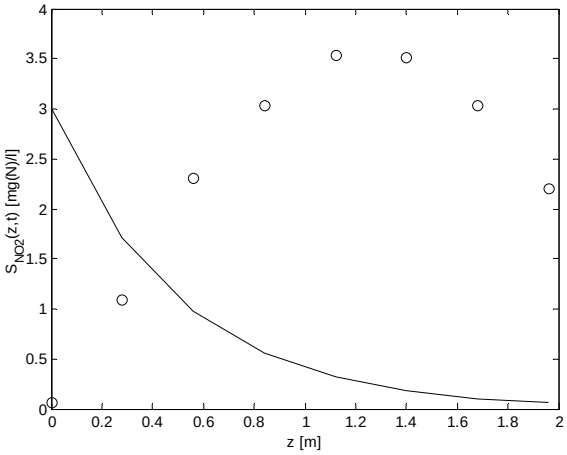

Fig. 7: Initial measured profile (circles) and exponential initial condition (solid line) of nitrite concentration.

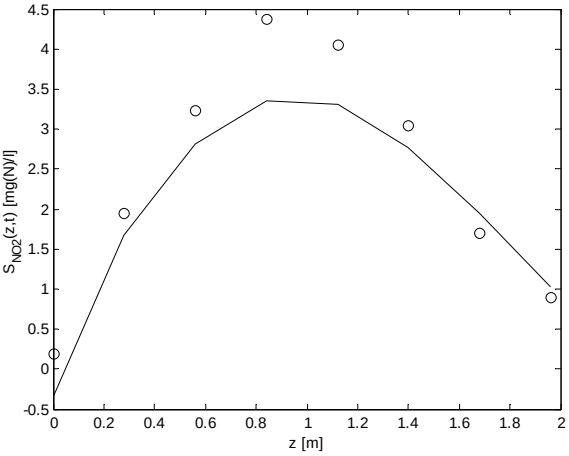

Fig. 8: measured profile (circles) and estimate (solid line) of nitrite concentration after 404 hours.

As the biomass distribution cannot be measured in practice, it is appealing to design a software sensor (or state observer) to reconstruct this information on-line. To this end, two options are considered: (a) an asymptotic observer, and (b) an exponential observer.

The asymptotic observer does not rely on the knowledge of the reaction kinetics, which is a decisive advantage with regard to the model uncertainties. However, the asymptotic observer appears unsuitable for the considered model structure, and an exponential observer, e.g. an extended Kalman filter or an extended Luenberger observer, is the only feasible solution. In this latter class of observers, receding-horizon (or full-horizon, when measurements are rare and corrupted by noises) observer provide a very simple, yet rigorous, solution to the nonlinear state estimation problem in distributed parameter systems with stochastic disturbances.

ACKNOWLEDGEMENTS

The authors are very grateful to the Laboratoire d'Ingénierie des Procédés de l'Environnement (LIPE) of INSA (Toulouse, France) for providing the experimental data.

REFERENCES

Allgöwer, F., Badgwell, T.A., Qin, J.S., Rawlings, J.B. and S.J Wright (1999). Nonlinear predictive control and moving horizon estimation - a introduction overview. In: *Advances in Control* (*Highlights of ECC'99*) (P.M. Frank, ed.), Springer-Verlag, 391-449.

Bascoul (1995). *Conduite Optimale d'un Biofiltre en Dénitrification d'Eau à Potabiliser*, Mémoire de DEA, Institut National des Sciences Appliquées de Toulouse, France.

Bastin, G. and D. Dochain (1990). *On-line estimation and adaptive control of bioreactors*, Elsevier, Amsterdam.

Bogaerts, Ph. and R. Hanus (2001). On-line state estimation of bioprocesses with full horizon observers, Mathematics and Computers in Simulation **56**, 425-441.

Bourrel S. (1996). *Estimation et Commande d'un Procédé à Paramètres Répartis Utilisé pour le Traitement Biologique de l'Eau à Potabiliser*, Ph.D. Thesis, Université Paul Sabatier, Toulouse, France.

Bourrel S., Dochain D., Babary J.P. and I. Queinnec (2000). Modelling; Identification and Control of a Denitrifying biofilter, *Journal of process Control* **10**, 73-91.

Dochain D. and P.A. Vanrolleghem (2001). *Dynamical Modelling and Estimation in Wastewater Treatment Processes*, IWA Publishing.

Henze M., Grady L., Gujer W., Marais G.R. and T. Matsuo (1987). *Activated sludge model Nr 1*, Technical report, IAWPRC Science and Technology Reports Nr 1, London.

Oh J., Yoon S.M., and J.M. Park (2001). Denitrification in Submerged Biofilters of Concentrated-Nitrate Wastewater, *Water Science and Technology* **43**, 217-223.

Vande Wouwer A., Renotte C., Queinnec I., Remy M. and P. Bogaerts (2002). Distributed parameter modeling of a fixed-bed biofilter with experimental validation, Proceedings of IEEE MED'02, Lisbon, Portugal.

Walter E. and L. Pronzato (1997). *Identification of Parametric Models from Experimental Data*, Springer – Masson.

AN OPTIMAL OPERATING STRATEGY FOR FED-BATCH FERMENTATIONS BY FEEDING THE OVERFLOW METABOLITE

S. Valentinotti [*], **C. Cannizzaro** [*], **B. Srinivasan** [**], **D. Bonvin** [**,1]

[*] *Laboratoire de Génie Chimique et Biologique*
[**] *Laboratoire d'Automatique*
Ecole Polytechnique Fédérale de Lausanne
CH - 1015 Lausanne, Switzerland

Abstract: Optimization of the fed-batch fermentation of *Saccharomyces cerevisiae* is analyzed. Due to the limited oxygen uptake capacity of the cells, the overflow metabolite ethanol is formed when the substrate concentration is above some critical value. This value decreases during the course of an experiment due to the reduction in dissolved oxygen concentration resulting from biomass formation. Optimal operation corresponds to regulating the substrate concentration along this time-varying critical value. This paper proposes a novel strategy to implement this optimal solution, whereby ethanol is fed along with the substrate and its concentration in the reactor regulated around the inlet concentration value. Sub-optimal strategies of practical interest are also discussed and simulation results are presented.

Keywords: Fed-batch fermentation, Overflow metabolite, Bottleneck principle, Optimization, Ethanol regulation.

1. INTRODUCTION

Biotechnology has risen to becoming one of the active research areas in the control community. In this work, the optimization of a key biotechnological process, the production of baker's yeast, is studied. Though presented for baker's yeast, the results are generally applicable to fermentation processes with microorganisms that present an overflow metabolism.

Numerous models have been proposed to describe the behavior of *Saccharomyces cerevisiae* under different growth conditions (Nielsen and Villadsen, 1994). The model used in this work was proposed by (Sonnleitner and Käppeli, 1986). It assumes that the oxidative capacity of *S. cerevisiae* is limited and constitutes a bottleneck in the oxidative metabolism. The size of this bottleneck may change from experiment to experiment and even during a given experiment due to changes in the cell metabolism, nutrient limitation, or other factors (van Hoek *et al.*, 1998). When the substrate uptake rate exceeds the oxidative capacity, the overflow metabolite ethanol is formed.

Maximization of biomass production is obtained when the glucose flux exactly matches the oxidative capacity of the cells. However, industrial bioreactors are often operated at substrate concentrations well under this critical value in order to avoid yield losses when substrate is transformed into ethanol, and/or accumulation of the overflow metabolite which might be toxic. This work proposes a methodology for ensuring optimality by operating the reactor at this unknown, time-varying critical value.

[1] Corresponding author: dominique.bonvin@epfl.ch

Regulating the concentration of the overflow metabolite has been used for the purpose of optimization in several works (Axelsson, 1989; Chen *et al.*, 1995; Valentinotti *et al.*, 2003). However, true optimality would require regulating the ethanol concentration at zero, which is not possible due to the non-zero resolution of the ethanol sensor. Thus, those approaches are at best sub-optimal.

In this work, the non-intuitive idea of adding the overflow metabolite in the feed stream is used. By choosing the ethanol regulation set point equal to its concentration in the feed, optimal operation can be achieved. The main advantage is that the sensor resolution is no longer a critical issue. Furthermore, if desired, sub-optimal operation can be obtained by adjusting the ethanol set point relative to its concentration in the feed.

The paper is organized as follows. In Section 2, a macroscopic process model is presented. Section 3 formulates the optimization problem and its nominal solution, while Section 4 discusses three on-line operating strategies. The adaptive control strategy is presented in Section 5 and simulation results are shown in Section 6.

2. PROCESS MODELING

A macroscopic description of the metabolism of *S. cerevisiae* fermentation includes the following reactions:

$$S + a_1 O_2 \overset{r_1}{\rightarrow} b_1 X + c_1 CO_2 \tag{1}$$

$$S \overset{r_2}{\rightarrow} b_2 X + c_2 CO_2 + d_2 P \tag{2}$$

$$P + a_3 O_2 \overset{r_3}{\rightarrow} b_3 X + c_3 CO_2 \tag{3}$$

where S is the substrate, P the reaction product ethanol that can also be oxidized by the cells, X the biomass, and CO_2 and O_2 carbon dioxide and oxygen, respectively. a_i, b_i, c_i, d_i and r_i are the yield coefficients and the reaction rate of the i^{th} reaction, respectively.

In this work, the overflow metabolism (bottleneck) model proposed by (Sonnleitner and Käppeli, 1986) is used. It assumes a limited respiratory capacity of the cells. The uptake of the glucose fed to the reactor is assumed to occur at the following rate:

$$r_s = k_s \frac{S}{S + K_s} \qquad \left[\frac{g \text{ of } S}{g \text{ of } X \;\; h}\right] \tag{4}$$

The rate at which the cells can oxidize the substrate is given by :

$$r_o = k_o \frac{O_2}{O_2 + K_o} \qquad \left[\frac{g \text{ of } O_2}{g \text{ of } X \;\; h}\right] \tag{5}$$

The rate r_o is seen as the bottleneck since it limits the amount of glucose that can be oxidized. Thus, Reaction (1) takes place as long as sufficient glucose and oxygen are available in the reactor. Its rate is determined by the smallest of the rates at which glucose and oxygen are taken up by the cells, r_s and r_o/a_1, respectively:

$$r_1 = \min\left(r_s, \frac{r_o}{a_1}\right) \tag{6}$$

The glucose concentration at which the oxidative capacity saturates is defined as S_{crit}, for which $r_s = r_o/a_1$. It follows that $S_{crit} = r_o K_S/(a_1 k_s - r_o)$ is a function of the dissolved oxygen concentration O_2. When the glucose flux is too large to fit through the bottleneck, *i.e.* $r_s > r_o/a_1$ corresponding to $S > S_{crit}$, the excess will overflow into the reductive metabolism resulting in ethanol production according to Reaction (2). This is in fact what gives this metabolism its name. The rate at which this reaction takes place is given by:

$$r_2 = \max\left(0, r_s - \frac{r_o}{a_1}\right) \tag{7}$$

If the glucose flux does not use up the whole oxidative capacity of the cells, the ethanol present in the reactor is oxidized simultaneously via Reaction (3). The excess oxidative capacity is given by $r_o - a_1 r_s$, and the rate at which ethanol is oxidized is therefore:

$$r_3 = \max\left(0, \min\left(r_p, \frac{r_o - a_1 r_s}{a_3}\right)\right) \tag{8}$$

$$r_p = k_p \frac{P}{P + K_p} \qquad \left[\frac{g \text{ of } P}{g \text{ of } X \;\; h}\right] \tag{9}$$

Based on the reaction model (1)-(3), the following macroscopic mass balances can be derived:

$$\frac{d(VX)}{dt} = (b_1 r_1 + b_2 r_2 + b_3 r_3) VX \tag{10}$$

$$\frac{d(VS)}{dt} = -(r_1 + r_2) VX + F S_{in} \tag{11}$$

$$\frac{d(VP)}{dt} = (d_2 r_2 - r_3) VX + F P_{in} \tag{12}$$

$$\frac{d(VO_2)}{dt} = k_L a V (O_2^* - O_2) - (a_1 r_1 + a_3 r_3) VX \tag{13}$$

$$\frac{dV}{dt} = F \tag{14}$$

where F is the substrate feed rate, V the volume, and S_{in} and P_{in} the inlet concentrations of S and P, respectively. The dissolved oxygen concentration in the bioreactor is given by (13), where $k_L a$ is the overall mass transfer coefficient, and O_2^* the dissolved oxygen equilibrium concentration. For simplicity, it is assumed that $k_L a$ and O_2^* remain constant throughout the experiment.

The model parameters are given in Tables 1 and 2, while the operating and initial conditions used in the simulation are provided in Table 3.

Parameter	Value	Unit
a_1	0.396	g of O_2/g of S
b_1	0.490	g of X/g of S
c_1	0.590	g of CO_2/g of S
b_2	0.050	g of X/g of S
c_2	0.462	g of CO_2/g of S
d_2	0.480	g of P/g of S
a_3	1.104	g of O_2/g of P
b_3	0.720	g of X/g of P
c_3	0.625	g of CO_2/g of P

Table 1. Yield coefficients for the proposed reaction mechanism.

Parameter	Value	Unit
k_s	3.500	g of S/g of X h
k_o	0.256	g of O_2/g of X h
k_p	0.170	g of P/g of X h
K_s	0.100	g of S/l
K_o	0.001	g of O_2/l
K_p	0.100	g of P/l

Table 2. Kinetic parameters for the rates r_s, r_o, and r_p.

Variable	Value	Unit
S_{in}	300	g/l
P_{in}	10	g/l
O_2^*	0.039	g/l
k_La	250	h^{-1}
V_{max}	8	l
F_{max}	3	l/h
X_o	1.5	g/l
S_o	0.023	g/l
P_o	10	g/l
O_{2_o}	0.039	g/l
V_o	4	l

Table 3. Operating and initial conditions

3. OPTIMIZATION PROBLEM AND NOMINAL SOLUTION

From a practitioner's perspective, the goal is to maximize the amount of biomass with minimum batch time, which in fact are two objectives in one. Thus, from an optimization perspective, these two objectives need to be combined. In this paper, the batch time is considered as the cost function to be minimized, and the biomass productivity as a constraint to be met. As a result, the optimization problem is formulated as follows: given operational constraints, determine the feeding strategy that minimizes the batch time while ensuring that the amount of biomass at final time is at least the prescribed quantity $(VX)_{des}$:

$$\min_{t_f, F(t)} \; J = t_f \tag{15}$$

subject to $(10) - (14)$

$$0 \le F(t) \le F_{max}$$

$$V(t_f) \le V_{max}, \; V(t_f)X(t_f) \ge (VX)_{des}$$

where t_f is the final time, V_{max} the maximal volume, F_{max} the maximum feed rate at which the substrate can be fed, and $(VX)_{des}$ the desired minimal amount of biomass computed as:

$$(VX)_{des} = V_o X_o + b_1 S_{in}(V_{max} - V_o) \tag{16}$$

which corresponds to the amount of biomass that can be attained from the substrate. Note that, due to the presence of ethanol in the feed, it is possible to produce slightly more biomass than $(VX)_{des}$. The optimal solution of (15) obtained numerically is shown in Figure 1.

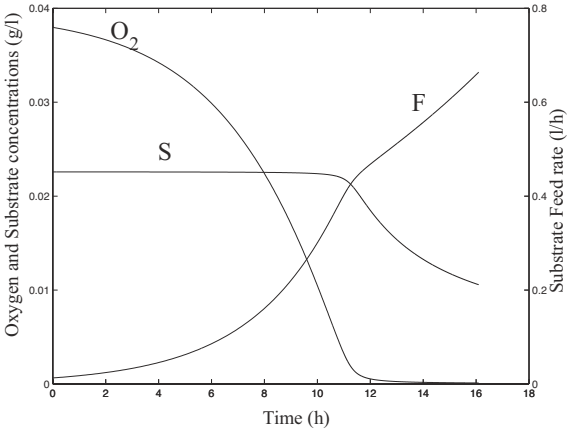

Fig. 1. Optimal feed rate profile and evolutions of oxygen and substrate concentrations.

It has been argued in Sonnleitner and Käppeli (1986) that exactly filling the bottleneck is optimal in some sense. Here, it will be shown that, for the optimization problem (15), the optimal solution in fact corresponds to exactly filling the bottleneck, i.e. regulating S at S_{crit}. To arrive at this conclusion, the two cases with $S \ge S_{crit}$ and $S \le S_{crit}$ are considered and it follows that $S = S_{crit}$ is indeed optimal.

- For $S \ge S_{crit}$, biomass is produced from the substrate by Reactions 1 and 2, and eventually the overflown ethanol is converted to biomass through Reaction 3. Thus, for the consumption of one unit of substrate, the quantity of biomass produced is $(b_1\alpha + (b_2 + d_2b_3)(1-\alpha))$, where $\alpha = r_1/r_s$, $0 \le \alpha \le 1$. Since $b_1 > (b_2 + d_2b_3)$, the maximum corresponds to $\alpha = 1$, i.e. $r_1 = r_s$ where the bottleneck is exactly filled. So, for $S > S_{crit}$, the desired productivity cannot be achieved with the substrate alone, and some of the ethanol in the feed stream must be consumed in order to produce the difference in the desired biomass production.
- For $S \le S_{crit}$, there is space in the bottleneck for some of the ethanol in the inlet to be converted to biomass, i.e. $r_3 = (r_o - a_1r_1)/a_3$. So, the rate of production of biomass is: $(\frac{b_1}{a_1}\beta + \frac{b_3}{a_3}(1-\beta))r_oXV$, where $\beta = a_1r_1/r_o$, $0 \le \beta \le 1$. Since, $\frac{b_1}{a_1} > \frac{b_3}{a_3}$, the maximum value is for $\beta = 1$, i.e. $r_1 = r_o/a_1$. In other words, the bottleneck should be entirely filled

with substrate in order to minimize time, though the desired productivity could be achieved even by partially filling it.

For the initial condition $S(0) = S_{crit}(O_2(0))$, the optimal input F^* that enforces $S = S_{crit}$ can be obtained by differentiating $r_s = r_o/a_1$ once with respect to time:

$$F^* = V\frac{N}{D}\bigg|_{S=S_{crit}} \tag{17}$$

where

$$N = a_1 K_o k_s S^2 (k_L a(O_2^* - O_2) - r_o X) + K_s k_o O_2^2 r_s X$$
$$D = a_1 K_o k_s S^2 O_2 + K_s k_o O_2^2 (S_{in} - S)$$

The first part of the feed rate profile is nearly exponential when oxygen is not limiting, while the second part is almost linear when oxygen limitation occurs after about 10 h. The optimal solution is $t_f^* = 16.12$ h. Figure 1 also indicates that S_{crit} reduces with time.

4. ON-LINE OPERATING STRATEGIES

Since the model parameters might not be accurately known and can vary during the batch, the feed rate expression (17) cannot be used to implement the optimal strategy. Instead, it is possible to use the ethanol concentration measurement P to adjust the substrate feed rate F.

As seen in the previous section, optimality requires $r_2 = r_3 = 0$, i.e. neither production nor consumption of ethanol. One possibility is to track the amount of ethanol $V(t)P(t) = (VP)_{ref}$ (Valentinotti *et al.*, 2003). Another possibility, which involves tracking the concentration of ethanol with $P_{in} \neq 0$, is discussed next.

Application of the chain rule of differentiation to (12) gives:

$$\frac{dP}{dt} = (d_2 r_2 - r_3)X + \frac{F}{V}(P_{in} - P) \tag{18}$$

Assume that P_{in} is constant and the ethanol concentration is regulated around the value P_{ref}. If $P(t) = P_{ref} = P_{in}$, then $dP/dt = 0$ implies $(d_2 r_2 - r_3) = 0$. However, since r_2 and r_3 are non-negative and cannot be positive simultaneously, $r_2 = r_3 = 0$.

In addition, depending on the relative values of P_{ref} and P_{in}, sub-optimal solutions are possible:

- $P_{ref} < P_{in}$ (for $r_2 = 0$ and $r_3 > 0$): Ethanol is constantly consumed and $S < S_{crit}$.
- $P_{ref} > P_{in}$ (for $r_2 > 0$ and $r_3 = 0$): Ethanol is constantly produced and $S > S_{crit}$.

The larger the difference $|P_{ref} - P_{in}|$, the more sub-optimal the operation will be.

Though it is preferable to keep the operation optimal, there might be biological reasons for choosing sub-optimal operation. Consider the optimal case where the ethanol concentration is regulated at P_{in}. Then, for any corrective action needed, for example, to reject a perturbation, the system has to switch from oxidative to reductive metabolism and vice-versa. In other words, if excess ethanol is produced, some space needs to be created in the bottleneck for it to be consumed. In contrast, this change of metabolism need not take place in sub-optimal strategies. Among the two sub-optimal strategies, $P_{ref} < P_{in}$ leads to $S < S_{crit}$, implying that maximal yield is still achieved, but the batch time is longer. On the other hand, $P_{ref} > P_{in}$ leads to shorter batch times at the cost of a reduction in yield.

The particular case $P_{in} = 0$ was considered in (Valentinotti, 2001). There, P_{ref} had to be as low as possible in order to be nearly optimal. Thus, P_{ref} was chosen based on the resolution of the ethanol sensor, which is no longer the case when a non-zero P_{in} is used. Furthermore, with $P_{in} = 0$, it is only possible to control the system in the overflow situation since negative concentrations cannot be measured. In contrast, with a non-zero P_{in}, the reference is shifted up to P_{in} and the system becomes observable and controllable for all three cases - overflow, critical, and underflow.

5. CONTROLLER DESIGN

In this section, a linear adaptive controller will be used to maintain the ethanol concentration P constant. Thus, the computation of a linear model will be discussed first, followed by the design of the adaptive controller.

5.1 *Linear model*

The bioreactor is operated in the fed-batch mode and hence has no steady-state operating point. However, for optimal operation, $P(t) = P_{in}$ and $S(t) = S_{crit}$. So, linearization will be around these optimal values for P and S while using averaged values for the others, e.g. $\bar{V}$ and $\bar{F}$.

In order to derive a linear model, it is assumed that (VS) is at quasi-steady state:

$$\frac{d(VS)}{dt} = -(r_1 + r_2)XV + FS_{in} = 0 \tag{19}$$

The linearized dynamics will be different depending on whether the second or the third reaction takes place in addition to r_1. Thus, two cases need to be considered:

- **Case A:** $r_2 \neq 0$**,** $r_3 = 0$**.** Here, $r_1 = r_o/a_1$ and, from (19), $r_2 X = (F/V)S_{in} - (r_o/a_1)X$. Using this expression in (18) leads to:

$$\frac{dP}{dt} = \frac{F}{V}(d_2 S_{in} + P_{in} - P) - \frac{d_2 r_o X}{a_1} \quad (20)$$

or, in linearized form:

$$\frac{dP}{dt} = -\frac{\bar{F}}{\bar{V}}P + \frac{d_2 S_{in} + P_{in} - P_{ref}}{\bar{V}}F \quad (21)$$
$$-\frac{\bar{F}}{\bar{V}^2}(d_2 S_{in} + P_{in} - P)V - \frac{d_2 r_o}{a_1}X$$

$$\frac{dV}{dt} = F \quad (22)$$

The linearized discrete-time model then reads:

$$P(kh) = \frac{B_1(q^{-1})}{A(q^{-1})}(F(kh) - w_1(kh)) \quad (23)$$

where $B_1 = \bar{B}_1(1 - (1 - e^{(\bar{F}/\bar{V})h})q^{-1})$, $A = (1 - q^{-1})(1 - (1 - e^{-(\bar{F}/\bar{V})h})q^{-1})$ and $w_1 = d_2 r_o X/(a_1 \bar{B}_1)$, with $\bar{B}_1 = (d_2 S_{in} + P_{in} - P_{ref})/\bar{V}$, h the sampling period, kh the sampling instant, and q^{-1} the backward-shift operator.

- **Case B:** $r_2 = 0$**,** $r_3 \neq 0$**.** Here, $r_1 = r_s$ and, from (19), $r_1 X = (F/V)S_{in}$. Furthermore, assuming that the excess oxidative capacity is small, i.e. $r_p > (r_o - a_1 r_s)/a_3$, one obtains $r_3 = (r_o - a_1 r_1)/a_3$, and thus $r_3 X = r_0 X/a_3 - (a_1/a_3)(F/V)S_{in}$. Using this last expression in (18) gives:

$$\frac{dP}{dt} = \frac{F}{V}(\frac{a_1}{a_3}S_{in} + P_{in} - P) - \frac{r_o X}{a_3} \quad (24)$$

Similarly, linearization and discretization lead to the following discrete-time model:

$$P(kh) = \frac{B_2(q^{-1})}{A(q^{-1})}(F(kh) - w_2(kh)) \quad (25)$$

where $B_2 = \bar{B}_2(1 - (1 - e^{(\bar{F}/\bar{V})h})q^{-1})$, $\bar{B}_2 = (a_1 S_{in}/a_3 + P_{in} - P_{ref})/\bar{V}$ and $w_2 = r_o X/(a_3 \bar{B}_2)$.

The following averaged linearized discrete-time model will be used:

$$P(kh) = \frac{B(q^{-1})}{A(q^{-1})}(F(kh) - w(kh)) \quad (26)$$

where $B = (B_1 + B_2)/2$ and $w = (w_1 + w_2)/2$.

Though the expressions for w_1 and w_2 are different, it is interesting to note that when $P_{ref} = P_{in}$, $w_1 = w_2$. In both linearized models, w is the input disturbance corresponding to the substrate flux needed for biomass growth. Since the biomass grows exponentially in the first phase and linearly in the second, the key problem is that of rejecting an *unstable* disturbance, for which standard PID-type controllers are inappropriate (Axelsson, 1989). Thus, an adaptive controller based on the internal model principle for disturbance rejection is used here (Valentinotti *et al.*, 2003).

5.2 *Adaptive controller design*

The RST polynomial control law with Q-parameterization is given by (Tsypkin, 1991):

$$R_o F = -S_o P + T P_{ref} - Q(AP - BF) \quad (27)$$

where R_o, S_o, and Q are polynomials in the backward-shift operator q^{-1}. The closed-loop characteristic polynomial is independent of the choice of Q and is given by $A_c = A\,R_o + B\,S_o$.

The resulting closed-loop system using the control law (27) is shown in Figure 2. The closed-loop output is given by:

$$P = \frac{BT}{A_c}P_{ref} - \frac{(Ro - Q\,B)}{A_c}w_B \quad (28)$$

with $w_B = Bw$ a filtered version of the disturbance w.

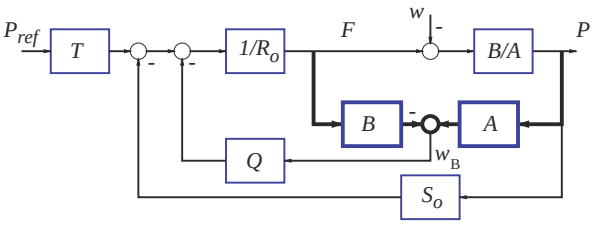

Fig. 2. Block diagram of the controlled system.

The goal of adaptation is to minimize the second term in (28) by adjusting Q:

$$\min_{Q} \ \|\epsilon_1 - \epsilon_2 Q\|^2 \quad (29)$$

where the signals ϵ_1 and ϵ_2 are defined as $\epsilon_1 = \frac{R_o}{A_c}w_B$ and $\epsilon_2 = \frac{B}{A_c}w_B$. Note that w_B can be estimated from the input and output using $\hat{w}_B(kh) = AP(kh) - BF(kh)$. Equation (29) corresponds to a linear regression problem for the elements of Q, for which on-line adaptation can be done using standard algorithms (Ljung, 1987).

6. SIMULATION RESULTS

The optimal and the two sub-optimal strategies proposed in Section 4 are implemented in simulation on the model presented in Section 2 using the controller described in Section 5. The substrate concentration and the feed rate for the various strategies are shown in Figures 3 and 4, and the numerical results are given in Table 4.

Strategy	P_{in}	P_{ref}	$X(t_f)$	$V(t_f)$	t_f
1	10	8	74.71	7.95	16.26
2	10	10	74.25	8.00	16.12
3	10	12	74.25	8.00	16.14

Table 4. Optimization results with the various strategies for $(VX)_{des} = 594$ *g*.

For the optimal Strategy 2, the substrate is always at its critical value $S_{crit}(O_2)$. Strategies 1 and 3

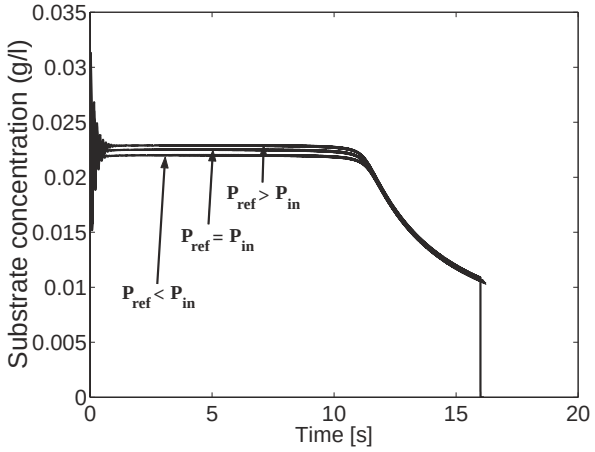

Fig. 3. Substrate concentration profile for various ethanol set points.

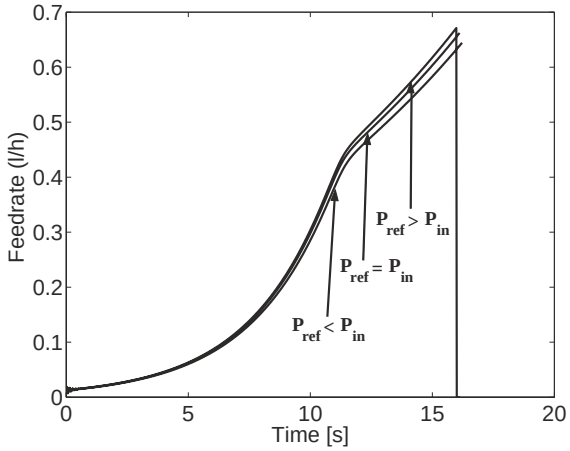

Fig. 4. Feed rate profile for various ethanol set points.

implement $S < S_{crit}$ and $S > S_{crit}$, respectively (see Figure 3).

For the case $P_{ref} < P_{in}$, since the bottleneck is not filled with substrate alone, part of the ethanol in the feed is converted to biomass. This way, a slightly higher $X(t_f)$ is obtained. Though the feed stops before the reactor is full, the final time is larger. On the other hand, when $P_{ref} > P_{in}$, there is overflow and the reactor is filled slightly faster. However, once the reactor is full, the productivity is less than the desired one. Thus, there is a small batch phase with $F = 0$ (see Figure 4) so as to produce the required biomass from ethanol.

As seen in Table 4, the minimal time is obtained with Strategy 2. Implementation is by regulating $P(t)$ around P_{in}. Note that no information regarding the model parameters is used in the controller, and the optimal solution is enforced solely from the ethanol measurement through feedback.

7. CONCLUSIONS

A non-intuitive approach for the optimal operation of fed-batch fermentations has been presented. This consists of adding a small amount of product in the feed solution and maintaining the product concentration in the fermenter constant at its inlet value.

The proposed operating strategy allows maintaining the desired metabolism (either overflow, critical or underflow) even when changes in the value of S_{crit} occur due to oxygen limitation. In fact, when the oxygen concentration is limiting, regulating P forces the substrate concentration S to decrease in order to match the oxidative capacity of the cells.

Although the analysis and the simulation study were done for *S. cerevisiae*, it is possible to use the proposed approached with other microorganisms presenting an overflow metabolism such as *E. coli*, a bacteria used for recombinant protein production.

8. REFERENCES

Axelsson, J. P. (1989). Modeling and Control of Fermentation Processes. PhD thesis. Lund Institute of Technology.

Chen, L., G. Bastin and V. van Breusegem (1995). A case study of adaptive nonlinear regulation of fed-batch biological reactors. *Automatica* **31**(1), 55–65.

Ljung, L. (1987). *System Identification. Theory for the User*. Prentice Hall.

Nielsen, J. and J. Villadsen (1994). *Bioreaction Engineering Principles*. Plenum Press. New York.

Sonnleitner, B. and O. Käppeli (1986). Growth of *Saccharomyces cerevisiae* is controlled by its limited respiratory capacity: formulation and verification of a hypothesis . *Biotechnology and Bioengineering* **28**, 927–937.

Tsypkin, Y.Z. (1991). Adaptive-invariant discrete control systems. In: *Foundations of Adaptive Control* (M. Thoma and A. Wyner, Eds.). Vol. 160 of *Lecture Notes in Control and Information Science*. pp. 239–268. Springer Verlag.

Valentinotti, S. (2001). Adaptive Rejection of Unstable Disturbances: Application to a Fed-batch Fermentation Process. PhD thesis No. 2045, Ecole Polytechnique Fédérale de Lausanne.

Valentinotti, S., B. Srinivasan, D. Bonvin, C. Cannizzaro, M. Rhiel and U. von Stockar (2003). Optimal operation of fed-batch fermentations via adaptive control of overflow metabolite. *Control Engineering Practice* **11**(6), 665–674.

van Hoek, P., J. van Dijken and J. Pronk (1998). Effect of specific growth rate on fermentative capacity of baker's yeast. *Applied and Environmental Microbiology* **64**(11), 4226–4233.

Target-set Control

R. K. Pearson
Daniel Baugh Institute for Functional Genomics and Computational Biology
Thomas Jefferson University
Philadelphia, PA, USA
B.A. Ogunnaike
Department of Chemical Engineering
and Center for Systems Biology
University of Delaware
Newark, DE, USA

Abstract

To survive in the face of uncontrollable natural variations, biological organisms have developed adaptation mechanisms that make them remarkably insensitive to variations in certain variables. Conversely, outside these ranges of admissible variation, biological function may change dramatically, usually in undesirable ways (e.g., the organisms die). As a consequence, a set-theoretic control strategy seems quite appropriate for biologically-based processes like fermentation reactors: many variables do not have to be controlled to precise setpoints, but they do have to be maintained within viable operating ranges. This paper proposes a strategy for this kind of set-theoretic control based on *zonotopes*, which are the images of n-dimensional cubes under affine transformations. This approach is well-suited to the control of linearized fundamental models or linear empirical models over a specified range of validity. In addition, the results presented here establish strong connections with classical linear control theory. Finally, these results are extended to *positive linear systems*, a class that includes many biological system models (e.g., compartmental models arising in pharmecokinetics) and that are inherently harder to control than unconstrained linear systems.

1 Introduction

This paper describes *target-set control,* a control strategy that leads to the selection of control input sequences that drive the system state vector into a specified target set. One motivation for target-set control is the control of biological processes and systems, where many variables must be kept within specified ranges, but variation within those ranges has little effect on system performance, due in part to the well-developed adaptive nature of biological organisms. For example, *homeostasis*, the term for the coordinated action by which living organisms maintain equilibrium and sustain life, has several distinguishing characteristics that are important to the engineer contemplating the control of biological systems:

1. Desired equilibrium conditions are generally in terms of ranges of acceptable values *not* precise point targets as is commonly the case in standard control engineering;

2. By design, intrinsic system robustness is achieved by ensuring that multiple combinations of input variable settings can equally well maintain the system at the desired equilibrium conditions. In other words, the problem of maintaining homeostasis has multiple equally admissible solutions. Contrast this with most standard control engineering problems for which non-uniqueness of a control solution may in fact be undesirable.

3. In their natural "settings", the states, inputs and output variables of typical biological systems are constrained to be non-negative at all times.

While one can definitely phrase the biological system control problem within the classical control theory framework (i.e. employ a model—often defined in terms of deviation variables—to compute a *unique* set of input variable values to drive system states to a unique set-point, subject to constraints), we believe that a more natural theoretical control framework for bioprocesses ought to take their distinguishing system characteristics into consideration explicitly.

2 Problem formulation

The basic problem formulation considered here is an extension of one considered previously [5], but based

on a more flexible class of uncertainty sets. More specifically, this formulation assumes the existence of an approximate linear model of the general form:

$$\mathbf{x}(k+1) = \mathbf{A}\mathbf{x}(k) + \mathbf{B}\mathbf{u}(k) + \mathbf{d}(k), \qquad (1)$$

where $\mathbf{x}(k)$ represents the n-dimensional state vector at time k, $\mathbf{u}(k)$ is the vector of m control inputs at time k, $\mathbf{A}$ and $\mathbf{B}$ are compatibly dimensioned matrices, and $\mathbf{d}(k)$ is an effective disturbance vector of dimension n. This model may be obtained by linearizing a fundamental model of process dynamics about some specified steady-state operating condition, via empirical model identification, or by any other means. The effective disturbance vector $\mathbf{d}(k)$ represents the combined effects on the state vector of linear model parameter uncertainty, neglected nonlinearities, discretization artifacts, and the influence of unmeasurable external disturbances. The control problem considered here is the following one:

> Given the process model (1), characterize the set of admissible sequences of control inputs $\{\mathbf{u}(k), \ldots, \mathbf{u}(k+r-1)\}$ that will drive the state vector $\mathbf{x}(k)$ into a designated target set S^* in R^n.

To solve this problem, we introduce the following sets:

- Σ_k, the set of all possible values for the state vector $\mathbf{x}(k)$ at time k,
- Δ_k, the set of all possible values for the effective disturbance vector $\mathbf{d}(k)$ at time k.

In what follows, given Σ_k, Δ_k, and a specific control input vector $\mathbf{u}(k)$, we first derive an expression for the set Σ_{k+1} of possible states $\mathbf{x}(k+1)$ and then extend this result to obtain an expression for the set Σ_{k+r} of possible values for $\mathbf{x}(k+r)$ for arbitrary $r \geq 1$. This multi-step result represents one important extension of our previous results [5]; another extension is the replacement of spherical uncertainty sets with more flexible *zonotopes*, described next.

3 Zonotopes

A zonotope is defined [8, p. 191] as the image of the p-cube under an affine projection map, where the p-cube is the set

$$C_p = \{\mathbf{x} \in R^p \mid |x_i| \leq 1,\ i = 1, 2, \ldots, p\}, \qquad (2)$$

and an affine projection of a set $\mathcal{A} \subset R^p$ is the set defined by

$$\mathbf{M} \bigotimes \mathcal{A} + \mathbf{b} = \{\mathbf{M}\mathbf{x} + \mathbf{b} \mid \mathbf{x} \in \mathcal{A}\}, \qquad (3)$$

where $\mathbf{M}$ is any $n \times p$ matrix and $\mathbf{b}$ is any vector in R^n. For convenience, let $Z_n(\mathbf{M}, \mathbf{b})$ denote the zonotope in R^n defined by:

$$\begin{aligned} Z_n(\mathbf{M}, \mathbf{b}) &= \mathbf{M} \bigotimes C_p + \mathbf{b} \\ &= \{\mathbf{x} \in R^n \mid \mathbf{x} = \mathbf{b} + \sum_{i=1}^{p} \lambda_i \mathbf{m}_i, \\ &\qquad |\lambda_i| \leq 1\}, \end{aligned} \qquad (4)$$

where $\mathbf{m}_i$ is the i^{th} column of the matrix $\mathbf{M}$. Note that if the matrix $\mathbf{M}$ is *diagonal*, the resulting zonotope is a *parallelepiped*, a rectangular polytope in R^p with its faces parallel to the coordinate axes.

To describe system evolution in terms of zonotopes, we need the following notion. The *Minkowski sum* of two sets $\mathcal{A}$ and $\mathcal{B}$ is defined by [8]:

$$\mathcal{A} \bigoplus \mathcal{B} = \{\mathbf{a} + \mathbf{b} \mid \mathbf{a} \in \mathcal{A},\ \mathbf{b} \in \mathcal{B}\}. \qquad (5)$$

Now, define Σ_{k+1}^0 as the set of all possible *unforced* states $\mathbf{x}(k+1)$, obtained by setting $\mathbf{u}(k) = 0$. This set is related to Σ_k and Δ_k by the evolution equation:

$$\Sigma_{k+1}^0 = [\mathbf{A} \bigotimes \Sigma_k] \bigoplus \Delta_k. \qquad (6)$$

To obtain results that are *computationally* useful from this general expression, it is necessary to specialize to a class of sets for which affine projections and Minkowski sums are easy to compute; zonotopes represent one such class.

More specifically, the zonotope $Z_n(\mathbf{M}, \mathbf{b})$ may be viewed as the Minkowski sum of p line segments in R^n, each defined by a column of the matrix $\mathbf{M}$, translated by the vector $\mathbf{b}$. That is,

$$\begin{aligned} Z_n(\mathbf{M}, \mathbf{b}) &= [\ell_1 \bigoplus \ell_2 \bigoplus \cdots \bigoplus \ell_p] + \mathbf{b} \\ \ell_i &= \{\mathbf{x} \in R^n \mid \mathbf{x} = \lambda \mathbf{m}_i,\ |\lambda| \leq 1\}. \end{aligned} \qquad (7)$$

It follows immediately from this result that the Minkowski sum of two zonotopes $Z_n(\mathbf{M}, \mathbf{b})$ and $Z_n(\mathbf{N}, \mathbf{c})$ is simply the Minkowski sum of the line segments defined by the columns of $\mathbf{M}$ and $\mathbf{N}$, offset by $\mathbf{b} + \mathbf{c}$. Defining the composite matrix $[\mathbf{M}\dot{:}\mathbf{N}]$ as

$$[\mathbf{M}\dot{:}\mathbf{N}] = [\mathbf{m}_1, \ldots, \mathbf{m}_p, \mathbf{n}_1, \ldots, \mathbf{n}_q], \tag{8}$$

the Minkowski sum of two zonotopes is given by

$$Z_n(\mathbf{M}, \mathbf{b}) \bigoplus Z_n(\mathbf{N}, \mathbf{c}) = Z_n([\mathbf{M}\dot{:}\mathbf{N}], \mathbf{b} + \mathbf{c}). \tag{9}$$

Hence, it follows that zonotopes are closed under Minkowski addition. To see that zonotopes are also closed under affine transformations, note that

$$\begin{aligned} \mathbf{A} \bigotimes Z_n(\mathbf{M}, \mathbf{b}) + \mathbf{c} &= \mathbf{A} \bigotimes [\mathbf{M} \bigotimes C_p + \mathbf{b}] + \mathbf{c} \\ &= [\mathbf{AM}] \bigotimes C_p + [\mathbf{Ab} + \mathbf{c}] \\ &= Z_n(\mathbf{AM}, \mathbf{Ab} + \mathbf{c}). \end{aligned} \tag{10}$$

4 State evolution

To describe state evolution under this framework, suppose that the initial state homeostatic set is $\Sigma_k = Z_n(\mathbf{V}_k, \mathbf{x}_k)$ for some $n \times p$ matrix $\mathbf{V}_k$ and some nominal state vector $\mathbf{x}_k$. Next, assume the uncertainty sets Δ_{k+j} associated with the effective disturbance vectors $\mathbf{d}(k+j)$ are $\Delta_{k+j} = Z_n(\mathbf{W}_{k+j}, \mathbf{d}_{k+j})$ where $\mathbf{W}_{k+j}$ is an arbitrary $n \times q_j$ matrix describing the uncertainty in $\mathbf{d}(k+j)$ about its nominal value $\mathbf{d}_{k+j}$. It follows from Eq. (6) that the one-step unforced state evolution is described by

$$\begin{aligned} \Sigma^0_{k+1} &= [\mathbf{A} \bigotimes Z_n(\mathbf{V}_k, \mathbf{x}_k)] \bigoplus Z_n(\mathbf{W_k}, \mathbf{d}_k) \\ &= Z_n([\mathbf{AV}_k\dot{:}\mathbf{W}_k], \mathbf{Ax}_k + \mathbf{d}_k). \end{aligned} \tag{11}$$

The control vector $\mathbf{u}(k)$ steers the center of the evolving uncertainty set, giving us the one-step state evolution equation

$$\begin{aligned} \Sigma_{k+1} &= \Sigma^0_{k+1} + \mathbf{Bu}(k) \\ &= Z_n([\mathbf{AV}_k\dot{:}\mathbf{W}_k], \mathbf{Ax}_k + \mathbf{d}_k + \mathbf{Bu}(k)). \end{aligned} \tag{12}$$

Iterating this result, it follows that the r-step state uncertainty set Σ_{k+r} is the zonotope $Z_n(\mathbf{V}_{k+r}, \mathbf{x}_{k+r})$, where

$$\begin{aligned} \mathbf{V}_{k+r} &= [\mathbf{A}^r\mathbf{V}_k\dot{:}\mathbf{A}^{r-1}\mathbf{W}_k\dot{:}\cdots\dot{:}\mathbf{W}_{k+r-1}] \\ \mathbf{x}_{k+r} &= \mathbf{A}^r\mathbf{x}_k + \mathbf{A}^{r-1}\mathbf{d}_k + \cdots + \mathbf{d}_{k+r-1} \\ &\quad + \mathbf{A}^{r-1}\mathbf{Bu}(k) + \cdots + \mathbf{Bu}(k+r-1). \end{aligned} \tag{13}$$

A useful rearrangement of this result is the following generalization of Eq. (12):

$$\Sigma_{k+r} = \Sigma^0_{k+r} + \Phi\mathbf{v}, \tag{14}$$

where Σ^0_{k+r} represents the r-step unforced evolution caused by the system dynamics (e.g., decay of initial conditions) and the influence of external disturbances. This term is given explicitly as

$$\begin{aligned} \Sigma^0_{k+r} &= Z_n(\mathbf{V}_{k+r}, \mathbf{y}_{k+r}), \\ \mathbf{y}_{k+r} &= \mathbf{A}^r\mathbf{x}_k + \mathbf{A}^{r-1}\mathbf{d}_k + \cdots + \mathbf{d}_{k+r-1}. \end{aligned} \tag{15}$$

The term $\Phi\mathbf{v}$ in Eq. (14) describes the influence of the control inputs applied over this time period:

$$\begin{aligned} \Phi &= [\mathbf{A}^{r-1}\mathbf{B}\dot{:}\cdots\dot{:}\mathbf{B}] \\ \mathbf{v} &= \begin{bmatrix} \mathbf{u}(k) \\ \vdots \\ \mathbf{u}(k+r-1) \end{bmatrix}. \end{aligned} \tag{16}$$

Note that $\mathbf{v} \in R^{rm}$ describes the complete sequence of control moves made in the r steps considered here, and that Φ is the $n \times rm$ controllability matrix.

5 Target-set control

Given the results just presented for uncertain state evolution, we require one more construct to address the control problem. The *Minkowski difference* between two subsets of R^n is defined by

$$\mathcal{A} \sim \mathcal{B} = \{\mathbf{x} \in R^n \mid \mathcal{B} + \mathbf{x} \subset \mathcal{A}\}. \tag{17}$$

It is important to note that the Minkowski difference is *not* the inverse of Minkowski addition; in particular, these operations are related by [6]:

$$(\mathcal{A} \sim \mathcal{B}) \bigoplus \mathcal{B} \subset \mathcal{A}, \tag{18}$$

where the inclusion is generally proper. To see the utility of this construct, suppose the control objective is to guarantee that the state vector $\mathbf{x}(k+r)$ lies in a specified target set S^*. The set of all possible "state corrections" that are consistent with this control objective is then given by

$$\begin{aligned}\Omega_{k+r} &= \{\mathbf{z} \in R^n \mid \Sigma^0_{k+r} + \mathbf{z} \subset S^*\} \\ &= S^* \sim \Sigma^0_{k+r}. \end{aligned} \tag{19}$$

Given the sequence of r control moves specified by the vector $\mathbf{v}$ and the r-step controllability matrix Φ, the set of *feasible* control moves that are capable of meeting our control objective is given by

$$\Upsilon_{k+r} = \{\mathbf{v} \in R^{rm} \mid \Phi\mathbf{v} \in \Omega_{k+r}\}. \tag{20}$$

Note that if Φ has rank n, the usual controllability condition [4, p. 460], $\Phi\mathbf{v}$ can assume any value in R^n, implying that the r-step control problem is feasible (i.e., the set Υ_{k+r} is not empty) if and only if the set Ω_{k+r} is not empty.

To determine the set Ω_{k+r}, first note that for any two sets $\mathcal{A}, \mathcal{B} \subset R^n$ and any two n-vectors $\mathbf{a}$ and $\mathbf{b}$,

$$[\mathcal{A} + \mathbf{a}] \sim [\mathcal{B} + \mathbf{b}] = [\mathcal{A} \sim \mathcal{B}] + [\mathbf{a} - \mathbf{b}], \tag{21}$$

so the Minkowski difference of two zonotopes becomes

$$\begin{aligned} Z_n(\mathbf{M}, \mathbf{b}) \sim Z_n(\mathbf{N}, \mathbf{c}) &= [Z_n(\mathbf{M}, \mathbf{0}) \sim Z_n(\mathbf{N}, \mathbf{0})] \\ &\quad + [\mathbf{b} - \mathbf{c}]. \end{aligned} \tag{22}$$

Next, suppose $\mathcal{P}$ is a parallelepiped in R^n and $\mathcal{Z}$ is an arbitrary zonotope in R^n. By the preceeding result, there is no loss of generality in assuming that both of these sets are centered at zero. Hence, the Minkowski difference between these sets may be written as

$$\begin{aligned}\mathcal{P} \sim \mathcal{Z} &= Z_n(\mathbf{M}, \mathbf{0}) \sim Z_n(\mathbf{N}, \mathbf{0}) \\ &= \{\mathbf{z} \in R^n \mid \mathbf{z} + Z_n(\mathbf{N}, \mathbf{0}) \subset Z_n(\mathbf{M}, \mathbf{0})\} \\ &= \{\mathbf{z} \in R^n \mid -M_{ii} \le z_i + y_i \le M_{ii}, \\ &\qquad \mathbf{y} \in Z_n(\mathbf{N}, \mathbf{0})\}. \end{aligned} \tag{23}$$

Next, note that any vector $\mathbf{y} \in Z_n(\mathbf{N}, \mathbf{0})$ may be written as

$$\mathbf{y} = \sum_{j=1}^{p} \lambda_j \mathbf{n}_j \;\Rightarrow\; y_i = \sum_{j=1}^{p} \lambda_j N_{ij}. \tag{24}$$

Applying the triangle inequality to this result gives

$$|y_i| \le \sum_{j=1}^{p} |\lambda_j||N_{ij}| \le \sum_{j=1}^{p} |N_{ij}|, \tag{25}$$

since $|\lambda_j| \le 1$ for all j. Further, the extreme values in this inequality are achievable by taking either $\lambda_j = \text{sign}\,\{N_{ij}\}$ or $\lambda_j = -\text{sign}\,\{N_{ij}\}$ for all j. Hence, the Minkowski difference result from Eq. (23) may be written more explicitly as

$$\begin{aligned}\mathcal{P} \sim \mathcal{Z} &= \{\mathbf{z} \in R^n \mid \\ &\qquad -M_{ii} + N^{\diamond}_{ii} \le z_i \le M_{ii} - N^{\diamond}_{ii}\}, \end{aligned} \tag{26}$$

where $N^{\diamond}_{ii}$ is defined as

$$N^{\diamond}_{ii} = \sum_{j=1}^{p} |N_{ij}|. \tag{27}$$

Defining the matrix $\mathbf{N}^{\diamond}$ as the $n \times n$ diagonal matrix with elements $N^{\diamond}_{ii}$, Eq. (26) may be written as

$$\mathcal{P} \sim \mathcal{Z} = Z_n(\mathbf{M}, \mathbf{0}) - Z_n(\mathbf{N}, \mathbf{0}) = Z_n(\mathbf{M} - \mathbf{N}^{\diamond}, \mathbf{0}). \tag{28}$$

Also, note that for the inequalities in Eq. (26) to be consistent—i.e., for the set $\mathcal{P} \sim \mathcal{Z}$ to be nonempty—it is necessary that $M_{ii} - N^{\diamond}_{ii} \ge 0$ for all i, meaning that the matrix $\mathbf{M} - \mathbf{N}^{\diamond}$ is positive semidefinite. Geometrically, this result means that the Minkowski difference between any parallelepiped $\mathcal{P}$ and any other zonotope $\mathcal{Z}$ is a parallelepiped.

In the context of the control problem of interest here, suppose each component of the state vector is constrained to lie in the interval $a_i \le x_i \le b_i$. This constraint corresponds to $\mathbf{x} \in S^* = Z_n(\mathbf{H}, \mathbf{x}^*)$ where the diagonal matrix $\mathbf{H}$ and the vector $\mathbf{x}^*$ are

$$H_{ii} = \frac{b_i - a_i}{2}, \quad x^*_i = \frac{a_i + b_i}{2}. \tag{29}$$

The set Ω_{k+r} is then given by

$$\begin{aligned}\Omega_{k+r} &= S^* \sim \Sigma^0_{k+r} \\ &= Z_n(\mathbf{H}, \mathbf{x}^*) \sim Z_n(\mathbf{V}_{k+r}, \mathbf{y}_{k+r}) \\ &= Z_n(\mathbf{H} - \mathbf{V}^{\diamond}_{k+r}, \mathbf{x}^* - \mathbf{y}_{k+r}). \end{aligned} \tag{30}$$

Further, note that this set is nonempty if and only if $\mathbf{H}_{ii} - [\mathbf{V}^{\diamond}_{k+r}]_{ii} \ge 0$ for $i = 1, 2, \ldots, n$. If these conditions hold, the set Υ_{k+r} of feasible controls defined

in Eq. (20) corresponds to the solution set for the following collection of n simultaneous inequalities:

$$\gamma_i^- \;\le\; [\Phi \mathbf{v}]_i \;\le\; \gamma_i^+, \tag{31}$$

where these bounds are given by

$$\begin{aligned} \gamma_i^- &= [\mathbf{x}^* - \mathbf{y}_{k+r}]_i - [\mathbf{H} - \mathbf{V}_{k+r}^{\diamond}]_{ii} \\ \gamma_i^+ &= [\mathbf{x}^* - \mathbf{y}_{k+r}]_i + [\mathbf{H} - \mathbf{V}_{k+r}^{\diamond}]_{ii}. \end{aligned} \tag{32}$$

Recall that for a controllable system, the controllability matrix Φ has rank n for $r \geq n$, from which it follows that any state correction in the set Ω_{k+r} is achievable. For a completely controllable system, the standard (i.e., non set-theoretic) solution would be to choose $\mathbf{v}$ so that $[\Phi \mathbf{v}]_i$ falls in the center of each interval defined in Eq. (31), corresponding to a set point for the state vector of $\mathbf{x}^* - \mathbf{y}_{k+r}$ and representing a standard disturbance rejection strategy. Conversely, note that if $\gamma_i^- \leq 0 \leq \gamma_i^+$ for $i = 1, 2, \ldots, n$, it follows that one feasible solution is $\mathbf{v} = \mathbf{0}$. This solution corresponds to the classical statistical process control (SPC) strategy: no control action is necessary so long as the controlled variables lie within their target specification. One advantage of the target-set formulation considered here is that it permits us to consider a range of alternatives between these two very different control strategies. This flexibility is particularly useful in connection with positive linear systems, as the following discussion illustrates.

6 Positive linear systems

Positive linear systems are linear systems whose states, inputs, and outputs are constrained to be nonnegative at all times. The local dynamics of biological systems can often be described by positive linear systems because the variables involved are concentrations, which cannot be negative. An important special case of positive linear systems are *compartmental systems*, which may be defined as systems composed of interconnected reservoirs and which correspond to asymptotically stable positive linear systems [3, p. 147]. It is important to note, however, that this positivity constraint applies to system models written in terms of absolute state variables and *not* to those written in terms of deviation variables about some specified steady-state, since such deviations can be either positive or negative. An important practical aspect of positive linear systems is that they are inherently harder to control than unconstrained linear systems; for example, controllability conditions are much more restrictive for positive linear systems [2]. An interesting feature of the results presented in the preceeding sections of this paper is that they extend directly to the case of positive linear systems and provide some additional insights into the differences between unconstrained and positive linear systems.

To obtain this extension to positive linear systems, first define the *positive p-cube:*

$$C_p^+ = \{\mathbf{x} \in R^p \mid 0 \leq x_i \leq 1,\ i = 1, 2, \ldots, p\}, \tag{33}$$

which is a subset of the *positive orthant of* R^n, denoted R_+^n. Next, define a *positive affine projection* of a set $\mathcal{A} \subset R_+^n$ as the set $\mathbf{M} \bigotimes \mathcal{A} + \mathbf{b}$, where $\mathbf{M}$ is an $m \times n$ matrix whose elements are all nonnegative and $\mathbf{b}$ is an m-vector whose components are all nonnegative. A *positive zonotope* is the subset of R_+^n denoted $Z_n^+(\mathbf{M}, \mathbf{b})$ and defined by any positive affine projection of the positive p-cube. It is not difficult to show that the Minkowski sum of positive zonotopes is a positive zonotope, and that any positive affine projection of a positive zonotope is another positive zonotope. As a consequence, all of the state evolution results (i.e., Eqs. (13) through (16)) carry over directly to positive linear systems: if the state vector lies in the set $Z_n^+(\mathbf{V}_k, \mathbf{x}_k)$ at time k, these equations describe its subsequent evolution in response to the unforced positive system dynamics, nonnegative disturbance inputs characterized by positive zonotopes $\Delta_{k+j} = Z_n^+(\mathbf{W}_{k+j}, \mathbf{d}_{k+j})$, and nonnegative control inputs $\mathbf{u}_{k+j}$.

The most important difference between the positive system formulation and the unconstrained formulation is that the set Ω_{k+r} defined by Eq. (30) does not lie in the positive orthant. Since nonnegative input sequences can generate only state vector changes in R_+^n for a positive linear system, we must restrict consideration to the positive part of Ω_{k+r}. As in the unconstrained case, it is easy to obtain an explicit expression for this set if the target set S^* is

a parallelepiped in R_+^n. Specifically, we have:

$$\begin{aligned}\Omega_{k+r}^+ &= [S^* \sim \Sigma_{k+r}^0] \cap R_+^n \\ &= [Z_n^+(\mathbf{H}, \mathbf{x}^*) \sim Z_n^+(\mathbf{V}_{k+r}, \mathbf{y}_{k+r})] \cap R_+^n \\ &= \{x \in R_n \mid 0 \le x_i \le H_{ii} - \sum_{j=1}^{p} [\mathbf{V}_{k+r}]_{ij} \\ &\quad + x_i^* - [\mathbf{y}_{k+r}]_i, i = 1, 2, \ldots, n\}. \qquad (34)\end{aligned}$$

Given this result, the set Υ_{k+r} of admissible control moves consists of all nonnegative vectors $\mathbf{v}$ satisfying the following conditions for $i = 1, 2, \ldots, n$:

$$0 \le [\Phi \mathbf{v}]_i \le x_i^* - [\mathbf{y}_{k+r}]_i + H_{ii} - \sum_{j=1}^{p} [\mathbf{V}_{k+r}]_{ij}. \quad (35)$$

Note that the set Υ_{k+r} is non-empty if and only if the right-hand side of Eq. (35) is nonnegative for all i. *Also, note that these conditions hold if and only if the SPC solution* $\mathbf{v} = \mathbf{0}$ *is feasible.* This observation provides a very natural reference case for target-set control of positive linear systems: given a performance measure of interest and any other feasible control strategy in Υ_{k+r}, how does its performance compare with that of the SPC strategy?

Finally, note that even if Ω_{k+r}^+ is non-empty and Φ^{-1} exists, it will generally *not* be possible to generate all of the positive state corrections in Ω_{k+r}^+ with nonnegative control input sequences $\mathbf{v}$. In particular, note that Φ is a matrix with all nonnegative entries: even if Φ is square and Φ^{-1} exists, this inverse is necessarily an *M-matrix*, which has *non-positive* off-diagonal elements [1, ch. 6]. Consequently, unless Φ is a diagonal matrix, there will be elements of Ω_{k+r}^+ that can only be reached using negative control inputs. In practice, diagonality of Φ is an extremely restrictive condition; one case where this occurs is for a diagonal $\mathbf{B}$ matrix, corresponding to the monomial matrix condition for controllability discussed by Coxson and Shapiro [2]. The contrast between this result and the unconstrained linear system result (i.e., that every state correction in Ω_{k+r} is achievable if Φ^{-1} exists) provides yet another illustration of the important practical differences between positive linear systems and unconstrained linear systems.

7 Summary

As one reviewer noted, the target-set control approach described here bears some important similarities to the geometric approach to control theory [7]. He further argued that geometric control theory is more powerful because it does not restrict consideration to zonotopes. While we agree with this argument, we also note that the restriction to zonotopes has important advantages, both computationally in the simple construction of explicit sets of admissible control values and conceptually, as in the connections between controllability and statistical process control noted in Sections 5 and 6.

References

[1] A. Berman and A.J. Plemmons, *Nonnegative Matrices in the Mathematical Sciences*, Academic Press, 1979.

[2] P.G. Coxson and H. Shapiro, "Positive Input Reachability and Controllability of Positive Systems," *Linear Algebra Appl.*, v. 94, 1987, pp. 35–53.

[3] L. Farina and S. Rinaldi, *Positive Linear Systems: Theory and Applications*, Wiley, 2000.

[4] H. Kwakernaak and R. Sivan, *Linear Optimal Control Systems*, Wiley, 1972.

[5] R.K. Pearson and B.A. Ogunnaike, "Geometric Model Predictive Control: A Practical Approach to Uncertain Industrial Processes," *IFAC'96 Preprints*, vol. M, 1996 IFAC World Congress, San Fransisco, July, 1996, pp. 49–54.

[6] R.Schneider, *Convex Bodies: The Brunn-Minkowski Theory*, Cambridge University Press, 1993.

[7] M.W. Wonham, *Linear Multivariable Control. A Geometric Approach*, Springer-Verlag, 1974.

[8] G.M. Ziegler, *Lectures on Polytopes*, Springer-Verlag, New York, 1995.